Interaction Note

Note 622

4 July 2011

Transient RF and Microwave Pulse Propagation in a Debye Medium (Water)

David C. Stoudt, Ph.D., Frank E. Peterkin, Ph.D., and Brian J. Hankla, Ph.D.
Directed Energy Technology Office
Electromagnetic and Solid State Technologies Division
Code B20 / Bldg 1470
Dahlgren Division, Naval Surface Warfare Center
Dahlgren, VA 22448-5100

ABSTRACT

The development of Ultra-Wide-Band high-power microwave devices that generate fast-rise-time high-power multi-cycle 100 MHz to 10 GHz pulses has led to increased concern about the biological effects and potential hazards of this type of EM radiation. One key to evaluating the hazards is to establish a thorough understanding of the evolution of the pulse in various dielectric media. Many workers have done model calculations of dispersive propagation in water (as a representative biological media) at microwave frequencies and below using a variety of techniques. All of the analyses indicate that a microwave pulse exhibits severe distortion as it propagates in water. Experimentally, there has been little published confirmation of the effects predicted by the numerous model calculations.

We examine the development of transient fields that result when short-duration radio frequency (RF) and microwave pulses propagate in a dielectric that can be described as a Debye medium. These transient fields are fundamentally similar to Brillouin precursors that occur at optical frequencies and propagate much farther than would be expected for the center frequency of the pulse. The medium we examine first is 16 MΩ-cm deionized water, for which the polarization response below 10^{11} Hz is well represented using a single-resonance Debye model. Low conductivity water exhibits a quadratically increasing absorption coefficient in the frequency range from 10 to 10^4 MHz. As a microwave or RF pulse propagates in water, the frequency dependent attenuation increases the relative contribution of the lowest frequency components, causing changes in both pulse amplitude and morphology. We present numerical calculations of the propagation behavior for a variety of ideal pulse-modulation envelopes with frequency content below 2 GHz. Experimental results for pulsed RF and microwave signals in deionized water are presented which confirm the behaviors predicted by the ideal calculations, both in amplitude and in characteristic features.

We have also generalized this approach to evaluate the propagation characteristics in water of salinity varying from S = 0.3 to S = 10, comparable to that found in coastal waters. Numerical calculations were performed using the full complex form of the relative dielectric constant. Based on the results of the model, a microwave pulse generator and water transmission line were constructed to verify the numerical predictions. Good agreement between theory and experiment was found for the temporal evolution of the propagating signal, with less satisfactory agreement for the amplitude development.

TABLE OF CONTENTS

LIST OF FIGURES

CHAPTER 1 - Introduction

The development of Ultra-WideBand (UWB) high-power microwave (HPM) devices which generate fast-rise-time high-power multi-cycle 100 MHz to 10 GHz pulses has led to increased concern about the biological effects and potential hazards of this type of electromagnetic (EM) radiation. The majority of research on the biological effects of EM radiation has involved continuous-wave (CW) interactions [1][2]. Researchers have recently begun to examine the propagation characteristics and bio-effects of short EM pulses in dispersive biological media [3][4][5][6][7]. A short pulse can be taken to be one in which the width is at most a few tens of cycles of the signal frequency, bounded by an arbitrary modulation envelope. There are a myriad of biological media, but water is usually chosen as a representative medium since it is the primary constituent of most organisms.

For our purposes, the studies of dispersive propagation can be separated into those at optical frequencies and those at microwave frequencies (10 GHz) and below. At optical frequencies, much work has centered on understanding propagation in media in which the dielectric response is described by a Lorentz oscillator model. This was the original interest of Sommerfeld and Brillouin when they investigated the behavior of the "forerunner" or "precursor" signals that bear their respective names [8]. Their ideas have been extensively examined and extended using asymptotic techniques by others, notably Oughston and Sherman [9]. Water is often used as the medium in these calculations because it exhibits several "Lorentzian" features in its dielectric response at optical frequencies.

Sommerfeld precursors result from the high-frequency content of the pulse spectrum and propagate at the speed of light in vacuum due to the finite polarization response of any medium at high enough frequencies. From a theoretical perspective, the Sommerfeld precursor is always present since any causal signal has infinite frequency content. Sommerfeld precursors and precursor-like features have been observed experimentally [10][11], but due to practical bandwidth limitations the signal is usually very small.

Brillouin precursors develop due to the low-frequency content of the pulse and their characteristics are more dependent upon the detail of the dispersion characteristic for the medium. In most calculations using the Lorentz model the Brillouin precursor arrives at a distant point after the Sommerfeld precursor but before the main body of the incident pulse. This occurs because the energy velocity in a Lorentz medium is frequency dependent and exhibits an asymmetric U-shaped dip at the resonance frequency of the oscillator. It is possible, however, to choose conditions such that the Brillouin signal arrives after the main body of the pulse [9].

We discuss the effects at optical frequencies because there is some overlap in the concepts of dispersive propagation. However, the work reported here is more concerned with propagation effects in water at microwave frequencies and below. The primary difference derives from the fact that water exhibits a permanent dipole dielectric response below 10^{11} Hz and is therefore better described by a Debye model than a Lorentz model.

Many workers have done model calculations of dispersive propagation at microwave frequencies and below. Hart [5] considered pulse shapes produced in a model consisting of a two-layered (muscle-bone) dielectric sphere at frequencies < 1 MHz. Most others have confined their analyses to pure water for simplicity and have been more interested in the frequency range between 1 and 10 GHz. Studies reported by Albanese, et.al. [3] and Hart [5] were based on analytically decomposing

the pulsed radiation into a Fourier series, propagating each frequency component individually into the dielectric medium, and summing the terms of the Fourier series to obtain the resultant pulse shape. Moten, et.al. [4] used the Fast Fourier Transform (FFT) to do the equivalent analysis. Roberts and Petropolous [7] used a Green's function approach to calculate asymptotic behavior. Blaschak and Franzen [12] used Fourier series techniques to examine propagation at both optical and microwave frequencies at variable incident angles. Oughstun et.al [13] have applied the asymptotic approach using a model of distilled water that incorporates both Debye and Lorentz dispersion characteristics. All of these analyses indicate that a microwave pulse exhibits severe distortion as it propagates in water.

Experimentally, there has been little published confirmation of the effects predicted by the numerous model calculations. Smith [14] reported results of pulsed signals propagated in distilled water, as well as solutions with sugar and/or salt added. He described behavior consistent with increased relative contribution of the low frequency components of the pulse, but his pulses were not typical of those used in model calculations and so are difficult to compare.

The numerical technique we report in this paper is simple in that we consider *only* the frequency-dependent absorption for low conductivity water dielectric. Our numerical results indicate that, for frequencies below about 2 GHz, the primary cause of the pulse distortion is the frequency-dependent absorption coefficient of pure water. Group-velocity dispersion appears to have little effect on the results. This determination was made using standard frequency-domain techniques. When the results of this approach were compared to those obtained by Albanese, et.al. [3] that include the effects of group-velocity dispersion in pure water, they are found to be identical. Alternatively, when a more generalized technique was then applied to saline water the dispersion effects on the wave packet *were* evident, although the magnitude of the signal dropped significantly as well.

In Chapter 2 we first review and summarize propagation and absorption of plane waves in a lossy dielectric half-space comprised of low conductivity water, through the use of Maxwell's equations. We examine the roles which the frequency dependent dielectric constant, and conductivity, of water play in determining the absorption characteristics, and show (as have others) that as a result water behaves as a smooth low pass filter with a depth dependent cutoff frequency. Next, we use a straightforward FFT technique to examine the pulse distortion that occurs during propagation for a variety of waveform types. We then describe what we believe is the first clear experimental confirmation of transient development behavior that matches the theory with excellent qualitative and quantitative accuracy.

In Chapter 3 we generalize this approach to evaluate the propagation characteristics in water of salinity varying from S = 0.3 to S = 10, comparable to that found in coastal waters. Numerical calculations were performed using the full complex form of the relative dielectric constant. We describe a microwave pulse generator and water transmission line experiment setup different than that used in the work of Chapter 2 and which was designed based on guidance from the modeling results. We then present results which show good agreement between theory and experiment for the temporal evolution of the propagating signal, with less satisfactory agreement for the amplitude development.

CHAPTER 2 - Propagation in Deionized Water

2.1 Numerical Calculations

To understand how EM fields propagate in a lossy material, we examine Maxwell's equations for a homogeneous, linear, causal, and isotropic medium. Assuming that the charge density in the medium is zero ($\rho=0$). Maxwell's equations can then be written:

$$\nabla x\, \mathrm{E} = -\frac{\partial\, \mathrm{B}}{\partial\, t}$$

$$\nabla x\, \mathrm{H} = \sigma\, \mathrm{E} + \frac{\partial\, \mathrm{D}}{\partial\, t} \tag{1}$$

$$\nabla \bullet \mathrm{D} = 0$$

$$\nabla \bullet \mathrm{B} = 0$$

where **E** is the electric field, **D** is the displacement given by $\mathbf{D}=\varepsilon\mathbf{E}=\varepsilon_0\varepsilon_r\mathbf{E}$ with ε_0 the permittivity of free space and ε_r the relative dielectric constant of the medium, **H** is the magnetic intensity, **B** is the magnetic field given by $\mathbf{B}=\mu\mathbf{H}=\mu_r\mu_o\mathbf{H}$ with μ_o the permeability of free space and μ_r the relative permeability of the medium, and σ the electrical conductivity. With the help of the vector identity given by $\nabla x \nabla x \mathbf{A} = \nabla x \nabla \cdot \mathbf{A} - \nabla^2 \mathbf{A}$, the expression for the propagation equation for **E** is given by:

$$\nabla^2\, \mathrm{E} = \mu\, \sigma\, \frac{\partial\, \mathrm{E}}{\partial\, t} + \mu\, \varepsilon\, \frac{\partial^2\, \mathrm{E}}{\partial\, t^2} \tag{2}$$

For sinusoidal fields, Eqn. 2 becomes

$$\nabla^2\, \mathrm{E} - j\omega\, \mu\, (\, \sigma + j\omega\, \varepsilon\,)\, \mathrm{E} = 0 \tag{3}$$

Equation 3 describes the propagation of a sinusoidal EM field in terms of the material parameters σ, μ, and ε. Water can be assumed to be non-magnetic, so $\mu = \mu_o$. Further, although the behavior of ε and σ can be quite complicated at optical frequencies, for frequencies below 10^{11} Hz the simple Debye model is sufficient. In a single-resonance Debye model, the frequency-dependent relative dielectric constant and the conductivity are given by [15]

$$\varepsilon_r = \varepsilon_\infty + \frac{\varepsilon_s - \varepsilon_\infty}{[\, 1 + (\, \omega T\,)^2\,]} \tag{4}$$

$$\sigma = \sigma_{DC} + \frac{(\, \varepsilon_s - \varepsilon_\infty\,)\, \omega^2\, \varepsilon_o T}{[\, 1 + (\, \omega T\,)^2\,]} \tag{5}$$

where ε_o is the permittivity of free space, the radian frequency $\omega=2\pi f$, f is the frequency in Hz, σ_{DC} is the ionic conductivity at low frequency, ε_s and ε_∞ are the low and high frequency limits, respectively, of the relative dielectric constant, and T is the time constant for thermal relaxation. For

pure water $\varepsilon_\infty = 5.5$ is approximately constant, but ε_s varies with temperature and is 80.1 at 20 ºC and 78.2 at 25 ºC. The relaxation time constant also changes with temperature, T=9.5x10^{-12} sec at 20 ºC and T=8.1x10^{-12} sec at 25 ºC. We use the 25 ºC values for calculating ideal behavior to be consistent with published literature, but we use the 20 ºC values to compare with our experimental data. The DC conductivity is taken to be 10^{-5} mho/m.

Figure 1 shows the relative dielectric constant and conductivity for pure water given by Eqns. 4 and 5 at both 20 and 25 ºC. The dielectric constant is essentially independent of frequency below 1 GHz and only changes appreciably above 2 GHz. The conductivity, however, begins to rise from the DC level between 1 and 10 MHz. The conductivity increases as the square of the frequency, changing by 4 orders of magnitude between 10 MHz and 1 GHz.
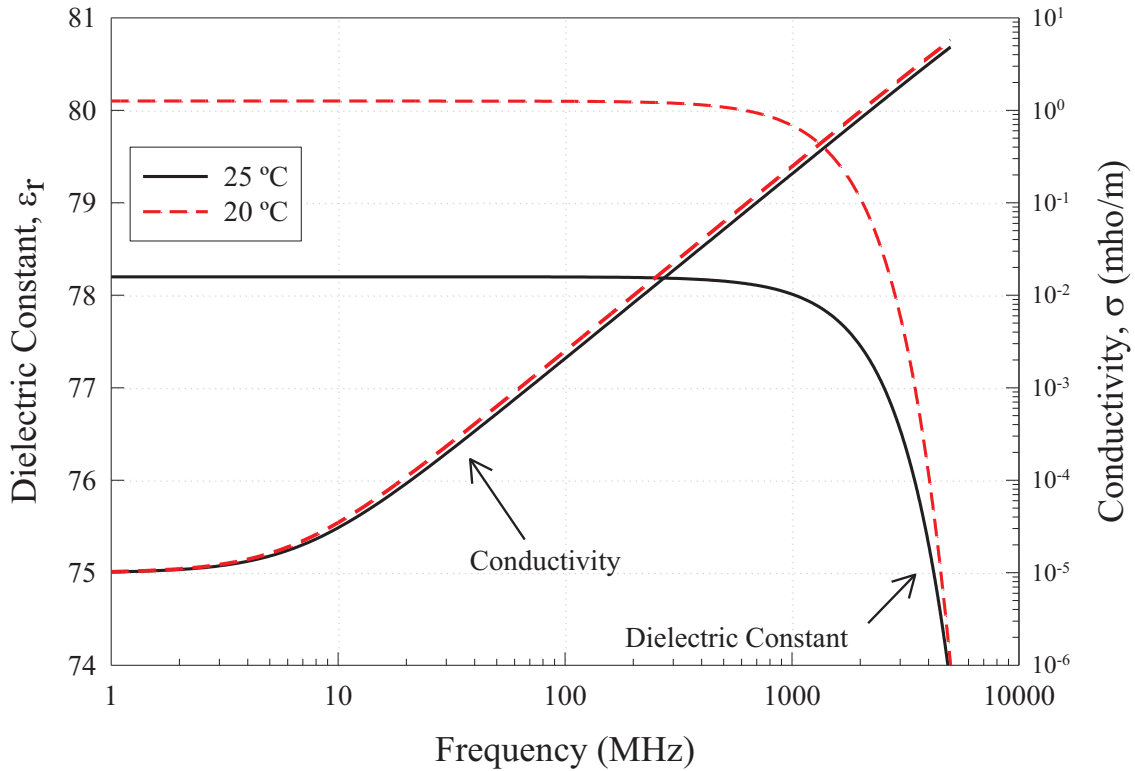
Figure 1 - Frequency dependence of the relative dielectric constant and electrical conductivity at 20 and 25 °C for deionized water using the Debye model parameters.

For a Transverse Electromagnetic (TEM) wave traveling in the z direction, a possible solution to Eqn. 3 in an infinite medium is given by

$$E(z,t) = E_o\, e^{-\gamma z}\, e^{j\omega t} = E_o\, e^{-\alpha z}\, e^{j(\omega t - \beta z)} \tag{6}$$

where γ is the propagation constant, the square of which is given by

$$\gamma^2 \equiv j\omega\mu(\sigma + j\omega\varepsilon) = (\alpha + j\beta)^2 \tag{7}$$

with α being the frequency-dependent absorption coefficient, and β the phase factor. Separating Eqn. 7 into its real and imaginary parts, we obtain the frequency-dependent expressions for α and β, which are given by Eqns. 8 & 9, respectively.

$$\alpha = \omega \sqrt{\frac{\mu\varepsilon}{2}\left(\sqrt{1 + \left(\frac{\sigma}{\omega\varepsilon}\right)^2} - 1\right)} \tag{8}$$

$$\beta = \omega \sqrt{\frac{\mu\varepsilon}{2}\left(\sqrt{1 + \left(\frac{\sigma}{\omega\varepsilon}\right)^2} + 1\right)} \tag{9}$$

Incorporating the expressions for ε and σ into Eqn. 8 enables us to plot the absorption coefficient of water modeled as a Debye medium $[\alpha(\omega) = f\{\omega, \sigma(\omega), \varepsilon(\omega)\}]$ as shown in Fig. 2a. At frequencies below 2 MHz the absorption coefficient is relatively independent of frequency, with a value of about 2×10^{-4} m^{-1}. Between 10 and 10^4 MHz the absorption coefficient varies as the square of frequency, increasing by 6 orders of magnitude. If we compare Fig. 2a with Fig. 7.9 in Ref. [16], we get very good agreement over the illustrated frequency range.

The frequencies that we are concerned with for this discussion are below 2 GHz. In this range we saw in Fig. 1 that the relative permittivity is nearly constant, so there will be little or no pulse dispersion resulting from a frequency-dependent propagation velocity. We conclude then that any distortion that an RF pulse exhibits, as a result of propagating in water, is solely due to frequency-dependent absorption.

We gain more insight into the effects of water on propagating EM fields by examining the attenuation as a function of depth. For a single frequency sinusoid, Eqn. 6 tells us that the attenuation, or the amplitude ratio of the field at a given depth to the field at z = 0, is given by a simple Beer's law relationship

$$\text{attenuation} = \frac{E(f, z)}{E(f, 0)} = e^{-\alpha(f)z} \tag{10}$$

Using the expression for α in Eqn. 8, Eqn. 10 is plotted in Fig. 2b in decibels for a set of propagation distances ranging from 0.75 to 10^4 meters at a water temperature of 25 ºC. It is readily apparent that the water behaves like a flat, lowpass filter with a depth-dependent cutoff frequency [4,12]. At 0.75 meters the -3 dB frequency is about 400 MHz, at 10 meters it is about 100 MHz, and by 1000 meters the cutoff occurs at about 7 MHz. The slope of the attenuation is also extremely steep. At 3 meters the cutoff frequency is around 200 MHz, but at that same depth the slope of the attenuation near 1 GHz is about -240 dB/decade. This is equivalent to a 12th-order filter function.

Figure 2b is the graphical representation of the foundation upon which we base our calculations. Below 2 GHz, pure water can be treated as a simple linear system. The curves in Fig. 2b are transfer functions for the system at various depths. We may thus use frequency domain techniques to find
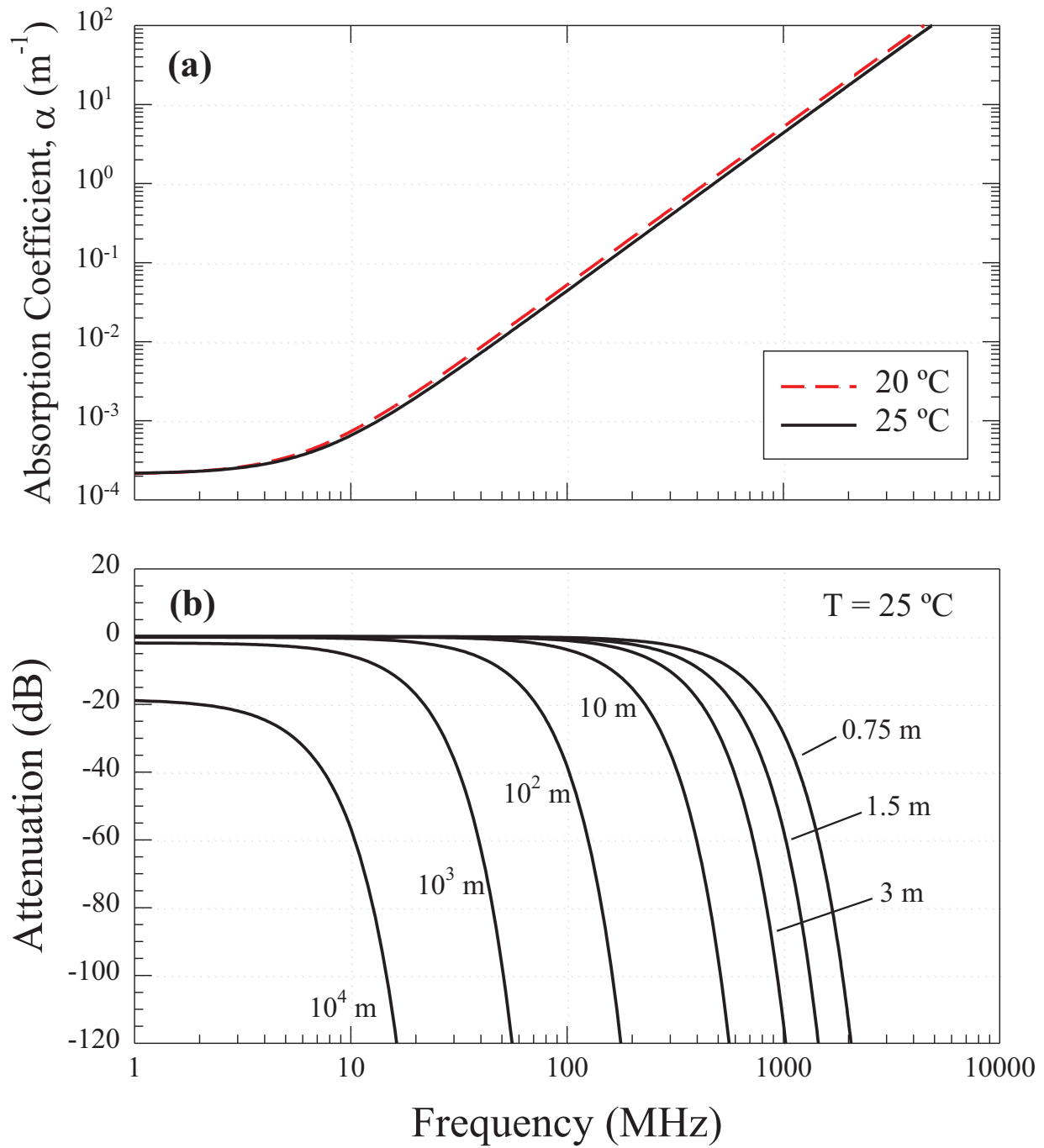
Figure 2 - (a) Frequency dependence of the absorption coefficient at 20 and 25 °C for deionized water using the Debye model parameters. (b) Attenuation in dB at 25 °C for depths ranging from 0.75 to 10^4 meters.

the effect of the water on input pulses. An input pulse is resolved into its component frequency distribution by taking the Fourier transform. The individual frequency contributions are scaled by the attenuation ratios shown in Fig. 2b for a given propagation distance. The inverse Fourier transform of the lowpass-filtered spectrum is then taken to generate the corresponding time-domain behavior of the pulse at the distance of interest.

The Fourier transform for an arbitrary pulse waveform can be difficult to describe in closed form. However, using discrete techniques it is possible to easily and rapidly calculate an approximation of the Fourier transform using the FFT. Briefly, given a continuous time domain signal x(t) discretely sampled at intervals Δt, the FFT is defined by [17]

$$FFT[x(n\Delta t)] = \widetilde{X}(k\Delta f\ ) = \sum_{n=0}^{N-1} x(n\Delta t)\, e^{-j2\pi n\Delta t k\Delta f} \tag{11}$$

where N is the number of sample points and must be an even power of 2, n and k are integer indices, and $\Delta f = 1/N\Delta t$. The FFT maps the set of sampled time domain points separated by spacing Δt into a complex valued image set in the frequency domain separated by spacing Δf. The approximation to the integral Fourier transform of x(t) is given by

$$\Im[x(t)]\big|_{f=k\Delta f} \approx \Delta t \cdot \widetilde{X}(f\ ) \tag{12}$$

Eqn. 12 states that the product of the sampling interval and the FFT gives approximate values for the Fourier transform of the continuous signal x(t) evaluated at discrete frequencies $f = k\Delta f$. Thus the FFT can be used to define the envelope of the Fourier spectrum.

Several points should be noted about using FFT methods to calculate Fourier transforms. The sampling frequency is given by $f_s = 1/\Delta t$. The sampling theorem limits the maximum frequency content of the time-domain signal which can be resolved to $f_s/2$, the Nyquist frequency. However, the frequency spacing in the FFT is determined by $\Delta f = f_s/N$. For a given sampled signal the bandwidth of the spectrum is fixed, but the resolution at which the spectrum is examined may be arbitrarily increased by simply padding the data with zeros to a higher power of 2. The only price is computational speed. We use padding extensively to better resolve our spectra.

The error, δ, in the approximation at a particular frequency $f = k\Delta f$ is given by the sum of the contributions at that frequency from each of an infinite number of replications of the transform spaced by f_s, or

$$\delta = \sum_{n=-\infty}^{n=\infty} X\,(k\Delta f - nf_s)\qquad n \neq 0 \tag{13}$$

where X(f) is the integral Fourier transform of x(t). Although not obvious by inspection, Eq. 13 implies that significant error may be present in the FFT representation of the Fourier transform, even for frequencies which are well below the Nyquist limit. The best way to reduce the error is to increase the sampling frequency (smaller Δt), which forces the replications of X(f) farther apart.

Numerical calculations were implemented with Visual Basic on a Pentium-class desktop computer. A typical calculation with frequency resolution of around 5 MHz for a time domain waveform

sampled at 50 ps required padding of the data to a total of 4096 points. Run times were of the order of a minute to follow the propagation dependence of a signal at 10 discrete distances.

We first examine the propagation characteristics of a square-modulated pulse and then discuss the effects of increasing the RF-pulse rise and fall times. In the calculations which follow, we pursue a slightly different approach than taken by most of the literature on this subject, which generally assumes a plane wave with unit-amplitude electric field incident on an air-water interface and then includes dielectric reflection as a loss. In the region of interest to us, the dielectric constant has essentially no frequency dependence, so reflection can be treated as a simple scaling factor. We wish to focus on the changes which occur during propagation, so all of the ideal calculations which follow are normalized to start with a unit amplitude signal which is at $z = 0^+$ (i.e. *already in the water)*.

Further, we describe our numerical results in terms of a voltage rather than electric field, anticipating our experiments that produce measured voltages on a transmission line. For TEM mode propagation in a transmission line, the electric field at any point is linearly related to the voltage by a geometric scale factor, so the qualitative behavior of the pulse distortion is unaffected by this approach.

It will be shown that our numerical analysis agrees exactly with comparable calculations obtained by others. This method does not *replace* more general analysis techniques that include group-velocity dispersion, as in Refs. [3-5], but it does show the *dominant* mechanism for RF-pulse distortion that occurs in pure water for frequencies below 2 GHz.

The intermediate propagation distances we highlight in the calculations are somewhat arbitrary. Some were chosen to facilitate direct comparison with the calculations of others in order to validate our numerical method. Others were chosen to highlight an interesting effect on the pulse. The final propagation depth for most of the ideal results is 3 meters to approximately correspond with our experimental arrangement.

2.1.1 Ideal square-modulated 1 GHz pulse

We begin by considering an ideal 10-cycle 1 GHz square-modulated pulse sampled at 50 ps intervals having a maximum amplitude of 1 V at $z = 0^+$, as shown in Fig. 3a. The shifted sinc-function amplitude-density spectrum (single sided) of this pulse is shown in the top trace of Fig. 3d to illustrate its frequency content both above and below 1 GHz. The nulls in the spectrum are not deep because the frequency resolution is limited to around 5 MHz by the number of points we chose to use in the calculation. More zero padding could have been used, but the computation time becomes excessive and no new information is provided.

Figure 3b shows how the pulse changes after propagating 0.75 m at 25 ºC. The pulse now exhibits leading and trailing transient peaks along with a weak remnant of the 1 GHz component. The transient peaks have an amplitude of about 0.2 V while the residual RF is down to only 0.03 V, a factor of 6 difference. This result is exactly equivalent to the comparable trace shown in Fig. 4 of Ref. [3] when the difference in methodology and the 79.7% air-water reflection coefficient are taken into account.
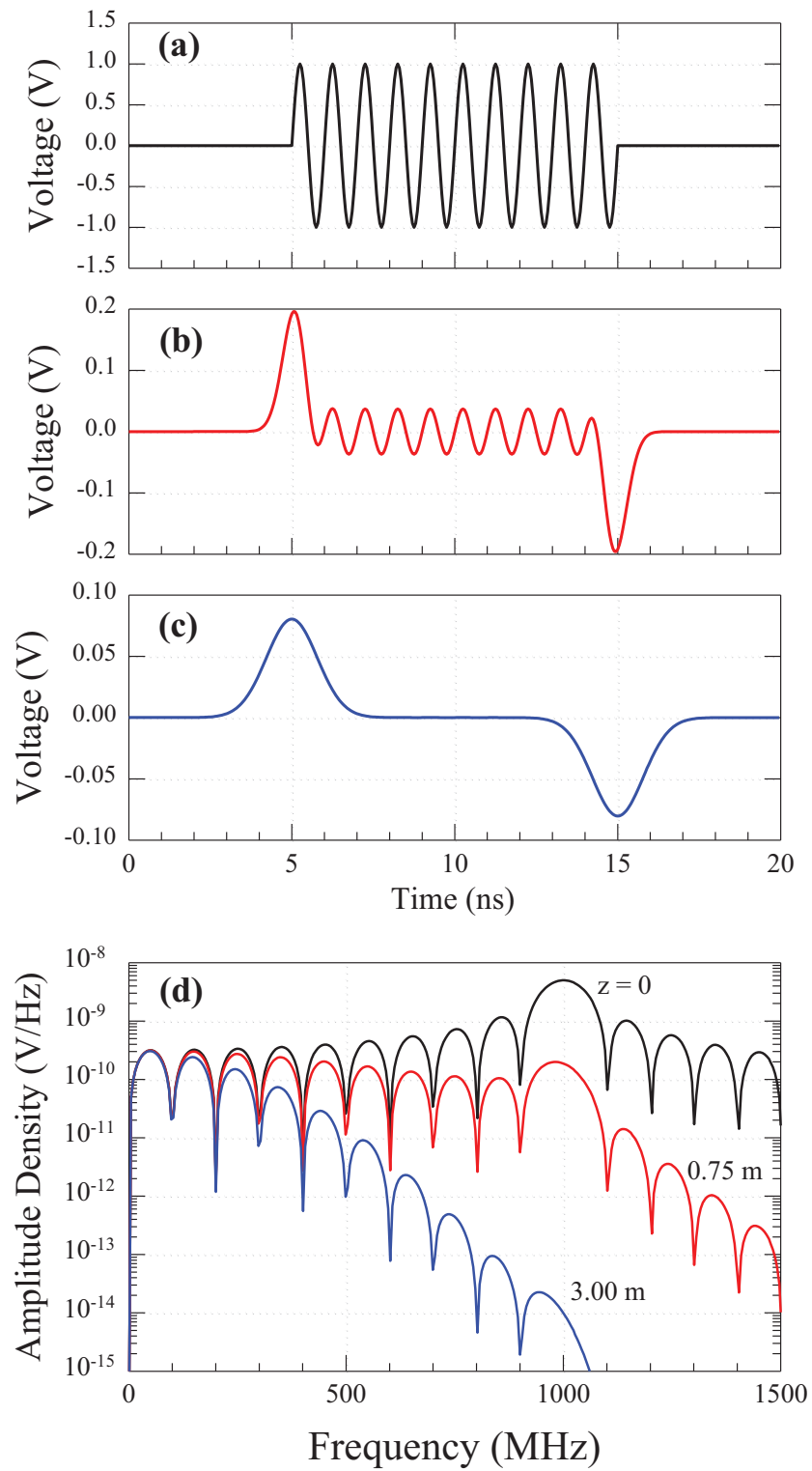
Figure 3 - Ideal 10 cycle, 1 GHz, square-modulated voltage pulse propagating in water at (a) zero (b) 0.75 m and (c) 3.0 m. (d) Amplitude-density spectra for all three pulses.

The transient peaks are also about 3 times wider than a half-cycle at 1 GHz, indicating the increased relative contribution of lower frequencies in this signal. Confirmation of this behavior is evident in the spectrum of this pulse, shown as the middle trace in Fig. 3d. We already see a significant effect due to the rapid rise of the absorption coefficient with frequency. Instead of an approximately symmetric sinc function, the central lobe at 1 GHz has been reduced to at or below the level of the lower frequency components. Frequencies above the fundamental are attenuated by at least 2 orders of magnitude. The spectrum below 500 MHz is hardly affected.

Figure 3c shows the pulse after propagating 3 meters. The transient peaks have decreased in amplitude to 0.08 V and have broadened to about 4 ns in duration. None of the 1 GHz fundamental signal is evident on this scale. Examination of the spectrum for this pulse (bottom trace of Fig. 3c) shows that the contribution from frequencies below about 200 MHz remains largely unaffected at this depth, but the fundamental lobe is now 4 orders of magnitude less than the lower frequency spectral peaks. Some care must be exercised when examining the results in Fig. 3a-c. Our numerical method calculates changes in pulse shape and amplitude due to frequency-dependent attenuation. It does not account for propagation velocity and so does not predict the time at which the pulse actually arrives at the depth of interest. The graphs of Fig. 3a-c are plotted on the same time scale because that is what the FFT method generates and it facilitates comparison of the developing changes. Since the dominant contributions to the pulse come from frequencies well below 2 GHz, the time of arrival for the various pulses can easily be calculated from the frequency-independent dielectric constant at a given temperature, as shown in Fig. 1.

When appropriate comparison is made between the results shown in Fig. 3 and those generated by Eqn. 3.12 in Ref. [3], we find that they are identical. These results are also in general agreement with those reported by Adair [18]. We are confident, therefore, in the validity of this calculation method, in interpretations we draw from the results, and in the extensions we make to different types of pulse forms not usually considered in the literature.

Using our calculation method, we find, as have others, that an ideal square-modulated 1 GHz pulse generates well-defined transients associated with the leading and trailing edges as it propagates into water. As pointed out by Albanese, et.al. [3], these transients resemble Brillouin precursors. Brillouin precursor fields do not experience exponential decay, but rather decrease with the propagation distance as $z^{-\frac{1}{2}}$ [19]. This fact could have significant impact on the determination of the biological effects of microwave fields. For example, if only the rapid absorption at 1 GHz is considered, any effect due to the lower frequency transients could be missed. This is particularly important since the dielectric relaxation frequencies of various bio-molecules lie between 100 MHz and 1 GHz, depending on the quantity and type of bound water molecules associated with them [15][20].

To examine this issue, the maximum amplitude of the propagating waveform for a pulse that starts as Fig. 3a is plotted as a function of depth in Fig. 4 (solid line). Also visible on Fig. 4 is the exponential decay (dash-dot line) we would expect from the 4.38 m^{-1} absorption coefficient at 1 GHz. It is readily apparent that after approximately one absorption length or 0.23 meters (inverse of absorption coefficient) the reduction in peak amplitude is no longer described by a simple exponential function,
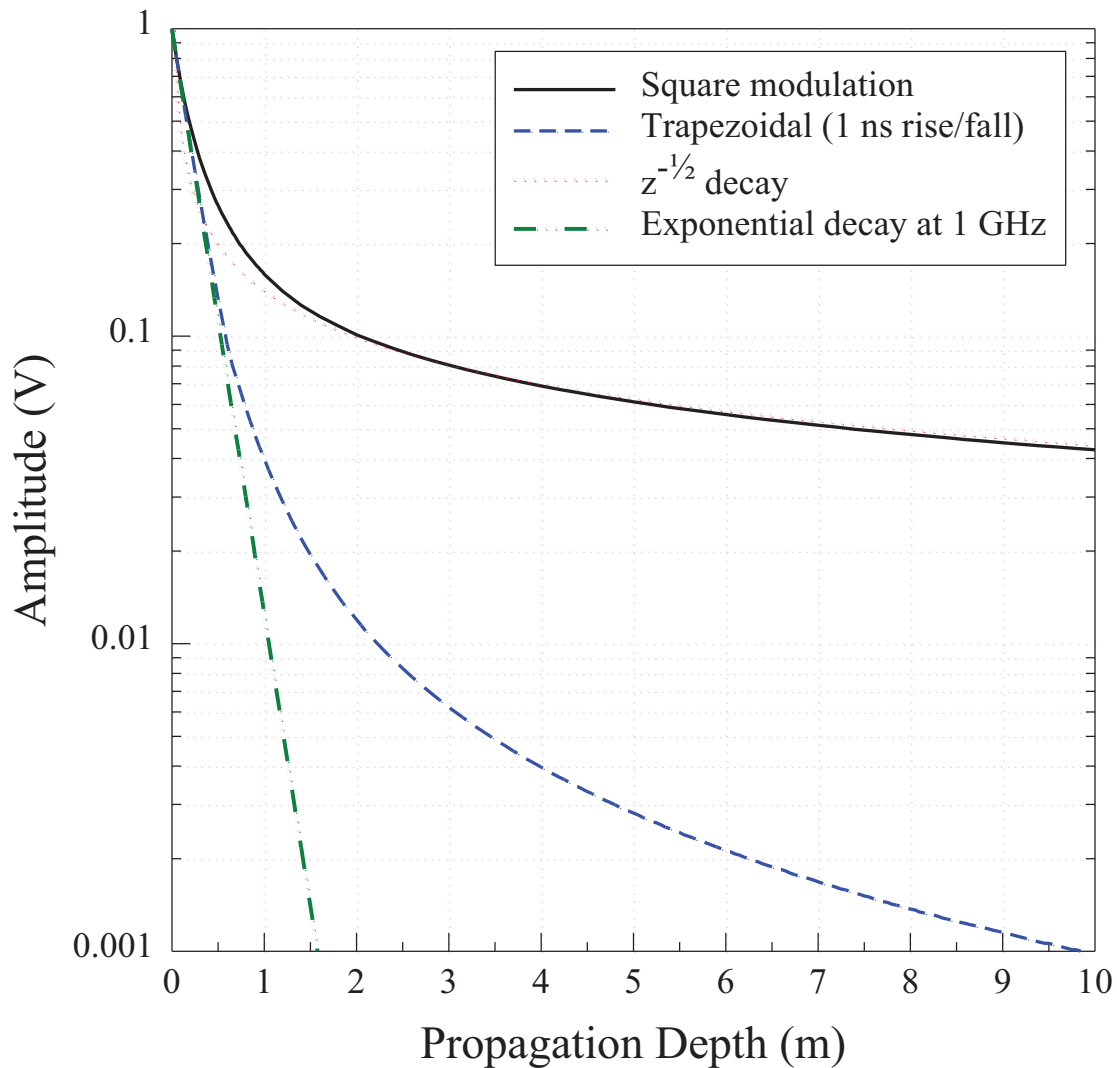
Figure 4 - Variation of the maximum transmitted amplitude as a function of distance for a 10-cycle 1 GHz pulse with square modulation (solid line) and trapezoidal modulation with 1 ns rise and fall time (dashed line). Also plotted are the expected exponential decay rate for a 1 GHz signal, and an inverse square root dependence arbitrarily scaled to best fit the square modulation curve.

and in fact is not related in any way to the original 1 GHz carrier. A fitted $z^{-\frac{1}{2}}$ dependence is also plotted on Fig. 4 (dotted line) and shows reasonable agreement in the range of 2 to 10 meters. A least-square curve fit of the exponent yields a better match using $z^{-0.566}$ (not shown).

From Fig. 2 we see that a plateau in the absorption coefficient occurs at a value of about 2×10^{-4} m^{-1} for frequencies below 5 MHz. The plateau extends down to 10 kHz before the absorption coefficient begins to decrease again. This plateau characteristic determines the pulse shape and attenuation at very great depth for a single pulse or pulses with Modulation Repetition Frequency (MRF) below 5 MHz. The inverse of the MRF is the time between modulated pulses.

This point is made more clear by examination of Fig. 2c. At depths greater than 1 km, the water behaves approximately as a low-pass filter with a cutoff frequency of 5 MHz and a depth-dependent attenuation in the pass band. At this depth, no shift in the relative contribution of significant remaining frequency components will occur, so the pulse shape stops changing. However, since each remaining frequency component is attenuated with the same exponential dependence, the entire waveform decays exponentially with the absorption coefficient of the plateau. The spectrum of a repetitively modulated pulse train is discreet. If the MRF is greater than 5 MHz, then the first harmonic is not within the plateau region. The higher order harmonics of such a signal will be attenuated significantly more than the first harmonic as the pulse travels to greater and greater depth. Since only one significant frequency-component remains in the spectrum, the waveform ultimately passes to a nearly single-frequency sinusoid at the MRF, regardless of the details of the modulation envelope or the carrier frequency. As discussed by Adair [18] and Moten [4], the depth dependence of a repetitive train of modulated pulses under these conditions thus passes asymptotically to the usual exponential form with an attenuation that is characteristic of the MRF.

2.1.2 Ideal 1 GHz pulse with trapezoidal modulation

We now turn our attention to the effect of increasing the rise and fall time of the modulation envelope. Termed trapezoidal modulation, the envelope of the pulse is determined by linearly rising and falling edges, with a flat central characteristic. Symmetric rising and falling behavior is usually assumed, although it does not have to be and interesting effects can be observed when it is not. This problem has been treated by several authors because it is still computationally tractable, and is in fact just the more general case of square modulation. We show that the changes in the transient fields that develop are again readily explained by frequency-dependent attenuation.

We consider a trapezoidally modulated 1 GHz pulse in water at $z = 0$ as shown in Fig. 5a. Here the RF pulse has a rise time (0-100 %) and a fall time (100-0 %) of 1 ns (one RF-cycle). As before, we show the Fourier spectrum of the trapezoidal pulse in Fig. 5d (top trace). Comparing with the square modulation spectrum in Fig. 3d, the high-frequency contributions are somewhat reduced, as would be expected. The amplitude of the fundamental lobe at 1 GHz is hardly affected by the risetime change. The low frequency composition, however, is dramatically different. The nulls in the spectrum have changed to a spacing of about 110 MHz. More significantly, the amplitude density below 200 MHz is 1 to 2 orders of magnitude lower than for the square modulation case. Note that this is an *amplitude spectrum*. Since the energy contained in a given frequency range varies as the square of the amplitude, there is much less energy available to form transients. Therefore, we would expect much lower amplitude transients.

Figure 5b shows the trapezoidal pulse after propagating 0.75 meters. There is indication of transient development at the leading/trailing edges, but not nearly to the level which was evident in Fig. 3b for otherwise identical conditions. The middle section of the pulse still displays the 1 GHz fundamental and is identical to Fig. 3b in that regard. Only when we follow the waveform more deeply do the transients become readily apparent. At 3 meters, in Fig. 5c, the fundamental component is no longer evident and a more complicated transient development than shown in Fig. 3c is observed. The major peak polarity has been inverted from the square modulation case, and the peak amplitude of about 6 mV is approximately one-third the value obtained for the square-modulation case. This inversion
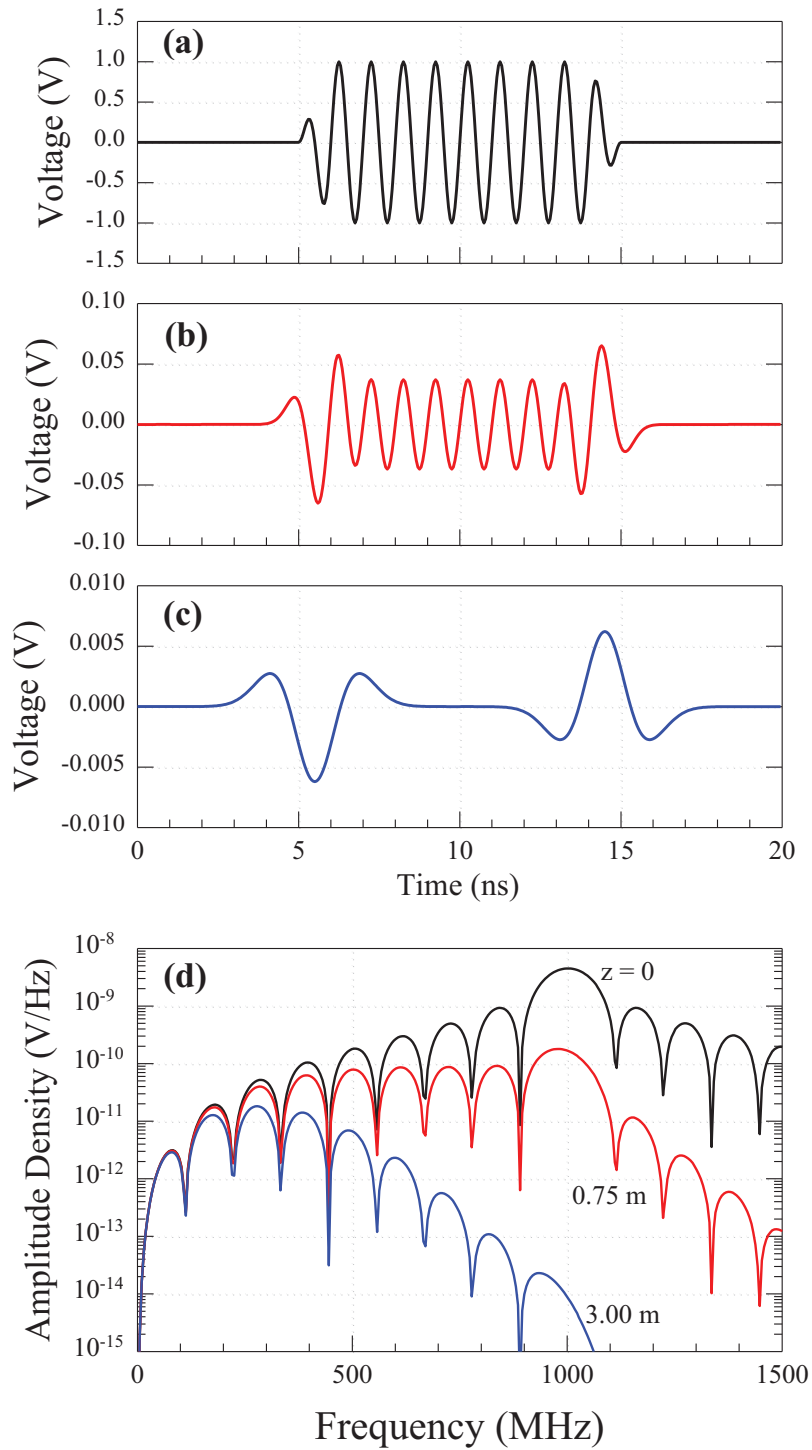
Figure 5 - Ideal 10-cycle, 1 GHz, trapezoidal-modulated voltage pulse with 1 ns rise and fall time propagating in water at (a) zero (b) 0.75 m and (c) 3.0 m. (d) Amplitude-density spectra for all three pulses.

has been noted by Albanese [3] as well for similar conditions. Again, the spectra of Fig. 5d show that the dominant contribution to the changing waveform comes from frequencies below 500 MHz.

The behavior of the maximum amplitude as a function of depth for trapezoidally modulated pulses has not been previously explored in great detail. The dashed line in Fig. 4 shows the variation of the peak amplitude for the pulse in Fig. 5a as it propagates. Initially, the peak falls off approximately exponentially as we would expect for 1 GHz. At about 0.5 meters, however, the curve begins to deviate and becomes noticeably non-exponential. Comparison with the dotted line in Fig. 4 shows that this variation is no longer approximately an inverse square-root dependence. A curve fit of the trapezoidal case for the range of 2 to 10 meters yielded a dependence varying approximately as $z^{-3/2}$.

From these results it is obvious that for a 1 GHz pulse, variations in the rise and fall time produces a continuum of transient decay parameters and behaviors. Albanese [3] showed that the leading and trailing edge transient shape shifted from a mono-pulse, to a quasi-monocycle, to an inverted polarity pulse, and finally to a double-cycle as the risetime/falltime of a 10-cycle 1 GHz pulse increased from zero to one and a half periods. The low-frequency content of the signal determines the changes in pulse shape and depth of propagation in a non-obvious fashion.

2.1.3 Ideal 400 MHz square and trapezoidal pulse-modulation

From the low-pass characteristics in Fig. 1c, we see that for a depth of 3 meters we would expect any signal with dominant frequency components above 200 MHz to be significantly affected. To examine an intermediate case and for convenience of comparison with experimental results reported below, Fig. 6 shows a 6-cycle square-modulated 400 MHz pulse as it propagates at 0, 1.5, and 3 meters. We see that some amplitude change and pulse broadening is evident at 1.5 m, but that little transient development has occurred. At 3 meters, however, broadened leading and trailing transients are apparent with levels about 28% of the original pulse. The peaks are a little more than twice the fundamental component in the middle of the pulse, and broaden the entire pulse from 15 to 19 ns.

Figure 7 shows the effect of trapezoidal modulation at 400 MHz. In Fig. 7a, we see the input pulse with 6 cycles and 2.5 ns (one RF cycle) risetime/falltime. The shape of the pulse at 1.5 meters (Fig. 7b) and 3.0 meters (Fig. 7c) exhibits some broadening, but remains almost undistorted when compared to the original. There is only slight evidence of a transient peak associated with the third and tenth RF half-cycles.

2.1.4 Pulses with DC components

The ideal pulse shapes considered previously have no average or DC component because they were chosen to have symmetric rise- and fall-time parameters with even numbers of RF half-cycles. However, the experiments we report below were performed on a coaxial transmission line, which supports TEM mode propagation with frequency content down to and including DC. Therefore, it is instructive to examine some of the waveforms with non-zero DC components which we have measured. From Eq. 8, the zero-frequency absorption coefficient is zero, so for the purposes of calculation the DC components were not attenuated regardless of the depth under consideration.
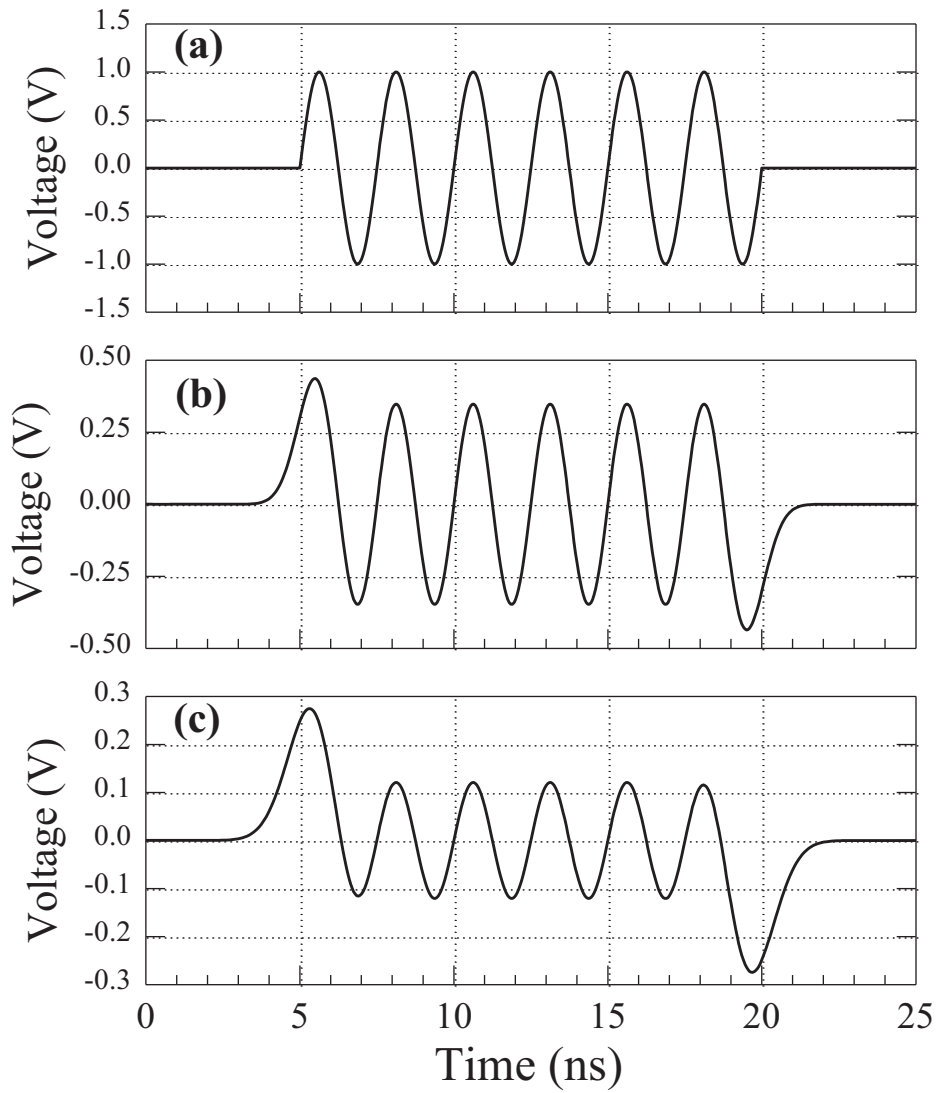
Figure 6 - Ideal 6-cycle, 400 MHz, square-modulated voltage pulse propagating in water at (a)
zero (b) 1.5 m and (c) 3.0 m.
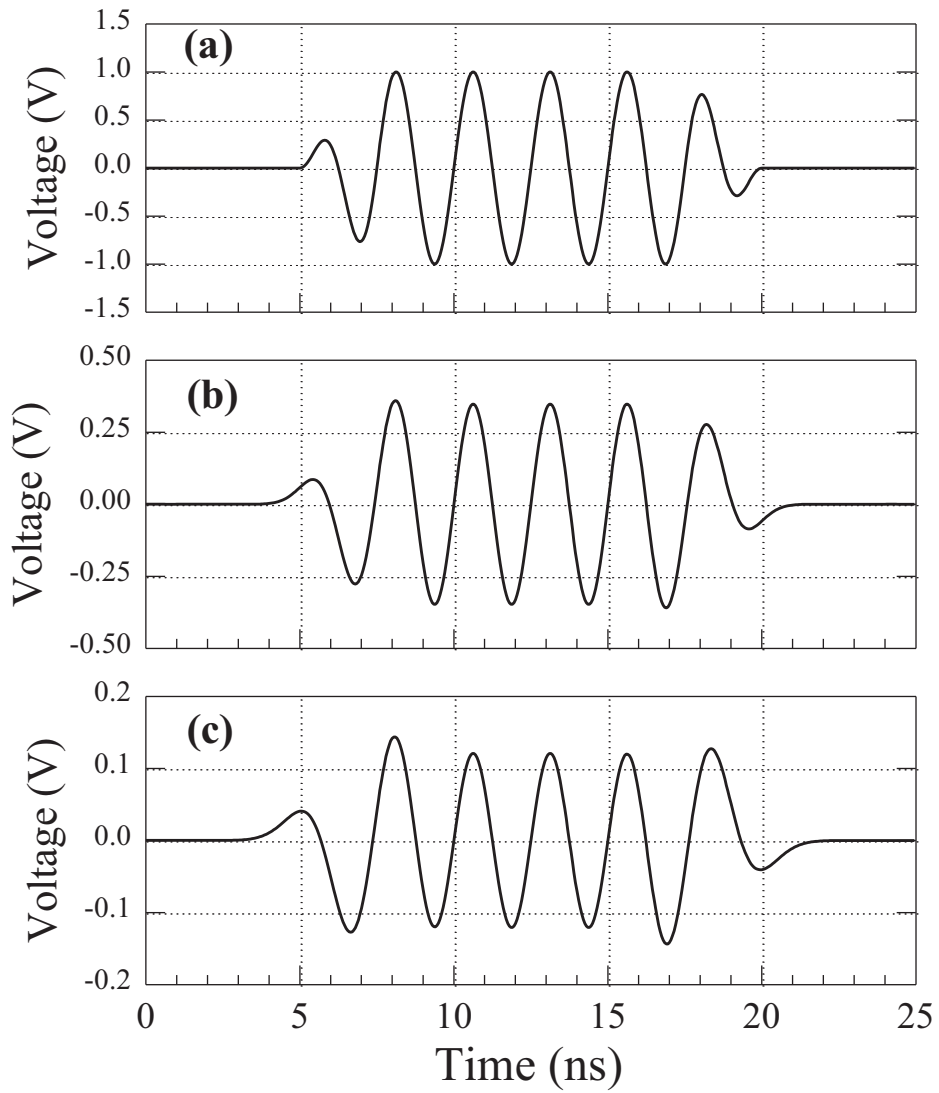
Figure 7 - Ideal 6-cycle, 400 MHz, trapezoidal-modulated voltage pulse with 2.5 ns rise and fall time propagating in water at (a) zero (b) 1.5 m and (c) 3.0 m.

The simplest pulse with a DC component is a square pulse. A 1 volt, 10 ns pulse is shown in Fig. 8a. Although ideally infinitely fast, this pulse has an effective rise/fall time of 50 ps due to the sampling interval used. The spectrum at z = 0 in Fig. 8d reflects the high DC content of this pulse. Given the lowpass-filter character of EM propagation in water, there are few surprises in the pulse development. At 0.75 meters, as shown in Fig. 8b, the pulse corners have been rounded off as the higher frequency components are attenuated, increasing the rise time to about 1 ns. At 3 meters, shown in Fig. 8c, the pulse has broadened further, with a risetime of greater than 2 ns. The peak voltage of the pulse remained unchanged at these depths.

Fig. 9a shows a variation of the square pulse in Fig. 8a, in which a 10-cycle 1 GHz sinusoidal modulation is superposed on a square pulse, again normalizing to unit peak-amplitude. The spectrum for this pulse shown in Fig. 9d exhibits two dominant peaks, one at DC and the other at 1 GHz. Fig. 9b shows the pulse after propagating 0.75 meters and is perhaps the most convincing of the examples we show for the dominance of the low-pass filter characteristic in determining waveform development at these frequencies. Little of the 1 GHz signal remains. The oscillation extremes have been damped or averaged to a value of about 0.5 volts, the DC level of the original pulse. This is somewhat different than the previous RF results, where in general the entire pulse was attenuated even as the shape evolved. At 3 meters, in Fig. 9c, there is no evidence that any 1 GHz contribution was ever present in this signal and it looks very much as if it had started as simply a square pulse.

Fig. 10a shows a 10.5-cycle square-modulated 1 GHz pulse, having positive first and last half cycles. The odd half-cycle number produces a DC component, evident in the spectra of Fig. 10d. At 0.75 meters the pulse has leading and trailing edge transient peaks which are both positive, as shown in Fig. 10b, along with some remainder of the 1 GHz fundamental. At 3 meters in Fig. 10c only the 2 positive transients are present. Comparing Figs. 10b and 10c with Figs. 3b and 3c we see that they are nearly identical except for the polarity of the trailing transients. Our calculations showed that for the four possible combinations of first and last half-cycle polarity with square modulation, the leading edge transient always follows the polarity of the first half-cycle of the initial pulse, while the trailing transient follows the polarity of the last half-cycle.

2.1.5 Extension to other modulation envelopes

We have identified the importance of the low-frequency components of trapezoidally modulated RF pulses (with square modulation as a special case) for the development and propagation of transient fields in a water dielectric. This analysis can readily be extended to other types of modulation schemes. For example, a Gaussian modulation in the time domain also yields a Gaussian envelope in the frequency domain. Similarly, a triangular modulation in the time domain contains very little low-frequency components. Therefore, both of these modulations, within the context of the above discussion, are not expected to yield substantial transient fields or variations in pulse shape. However, the slope of the effective lowpass filter function of the water is so steep that it tends to skew the peaks of the fundamental lobes (see for example Fig. 3d at 3 meters) so the frequency of the pulse is shifted to lower values.
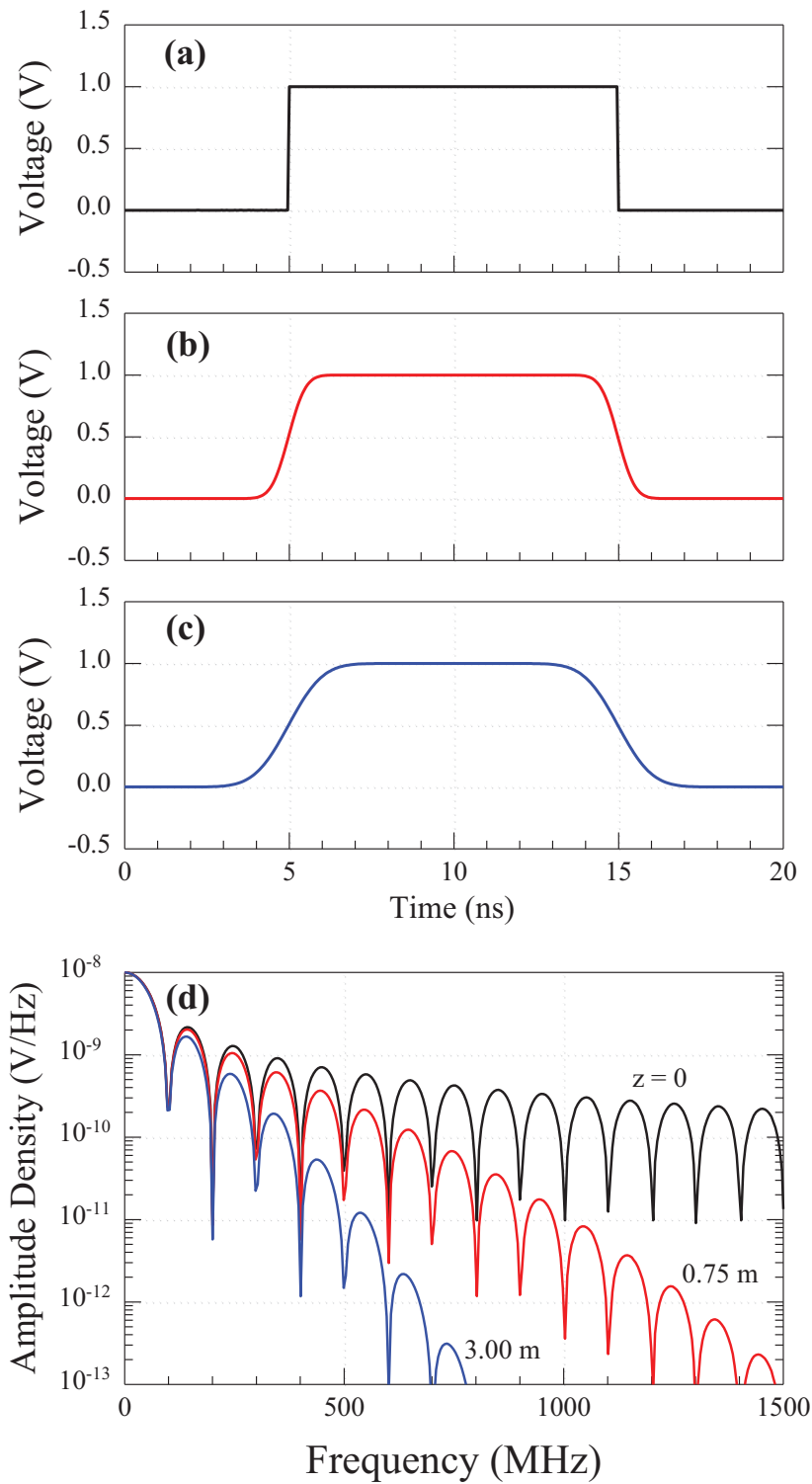
Figure 8 - Ideal 10 ns square voltage pulse propagating in water at (a) zero, (b) 0.75 m and (c) 3.0 m. (d) Amplitude-density spectra for all three pulses.
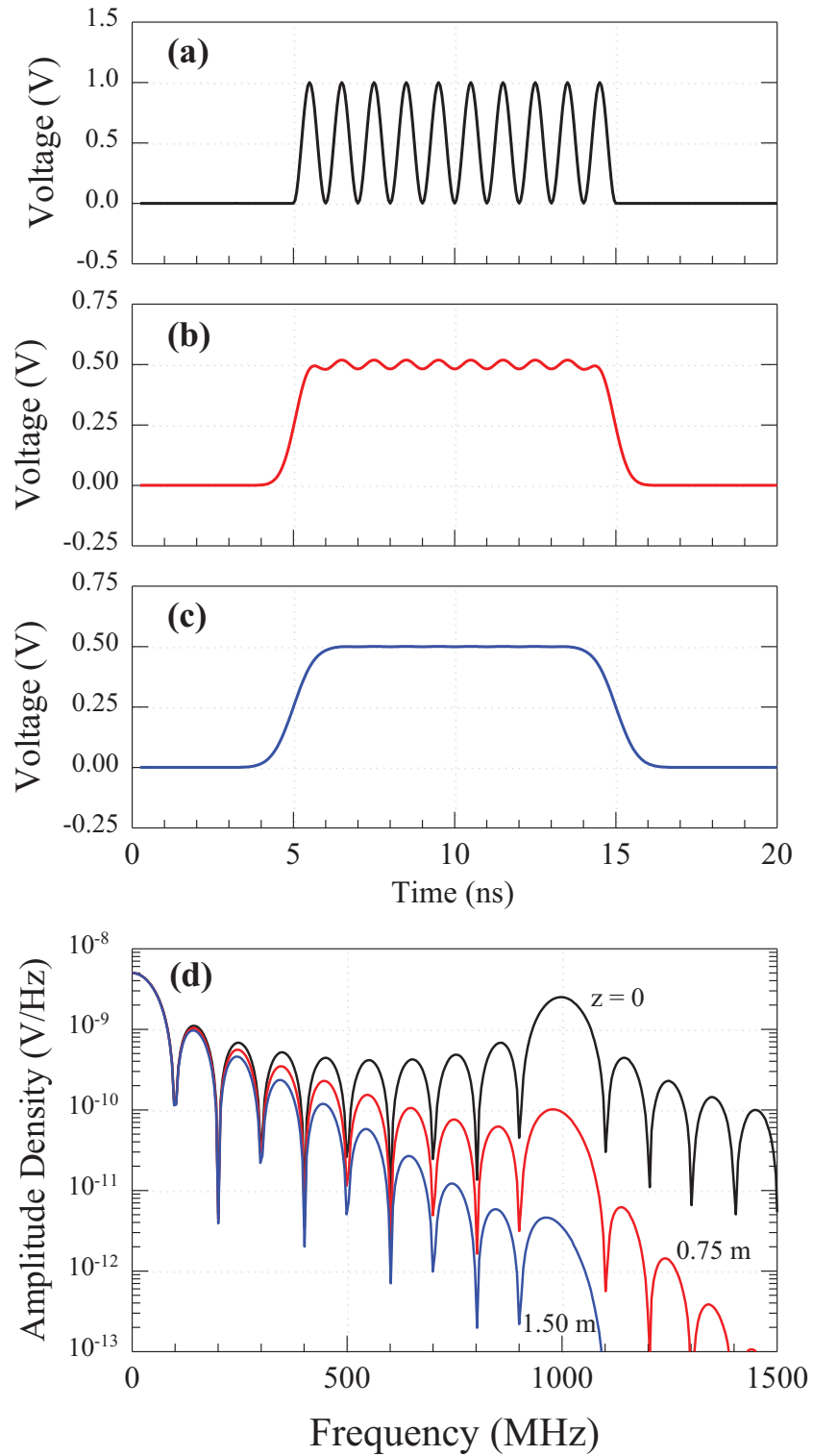
Figure 9 - Ideal 10 ns, offset, 1 GHz voltage pulse propagating in water at (a) zero, (b) 0.75 m
and (c) 1.5 m. (d) Amplitude-density spectra for all three pulses.
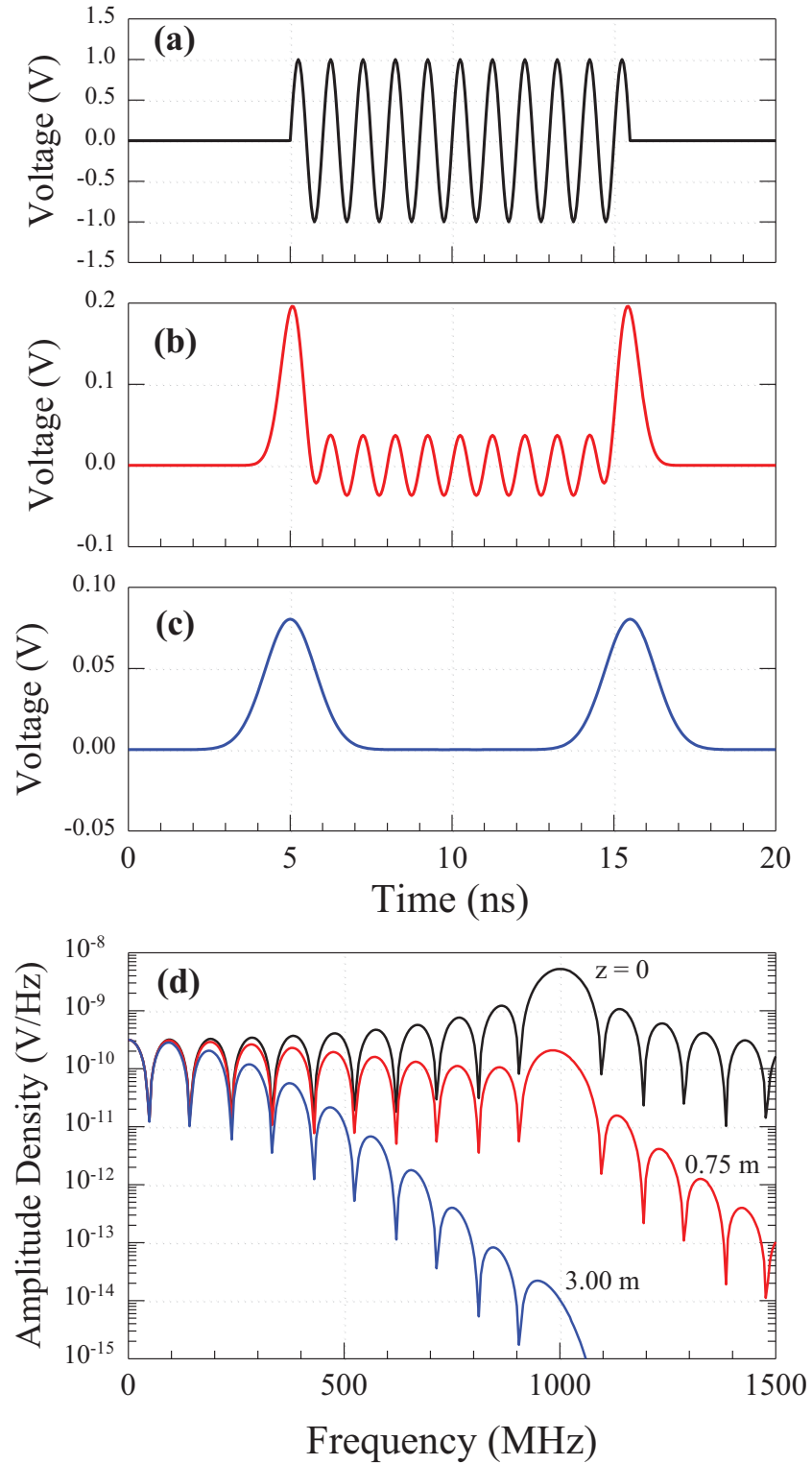
Figure 10 - Ideal 10.5-cycle, 1 GHz, square-modulated voltage pulse propagating in water at (a) zero (b) 0.75 m and (c) 3.0 m. (d) Amplitude-density spectra for all three pulses.

2.2 Measurements

2.2.1 Setup and method

To measure the changes in amplitude and morphology for each of the ideal pulse types discussed above, experiments were conducted using a propagation test cell filled with deionized water, shown schematically in Fig. 11. The test cell was a coaxial transmission line constructed from joined sections of stainless-steel Conflat-flange vacuum pipe four inches in diameter. A coaxial geometry was selected because of the relatively flat frequency response down to and including DC and because it supports TEM mode, providing a good approximation to a plane wave propagating in an infinite dielectric. For all experiments reported here the physical length of the cell was 1.38 meters.
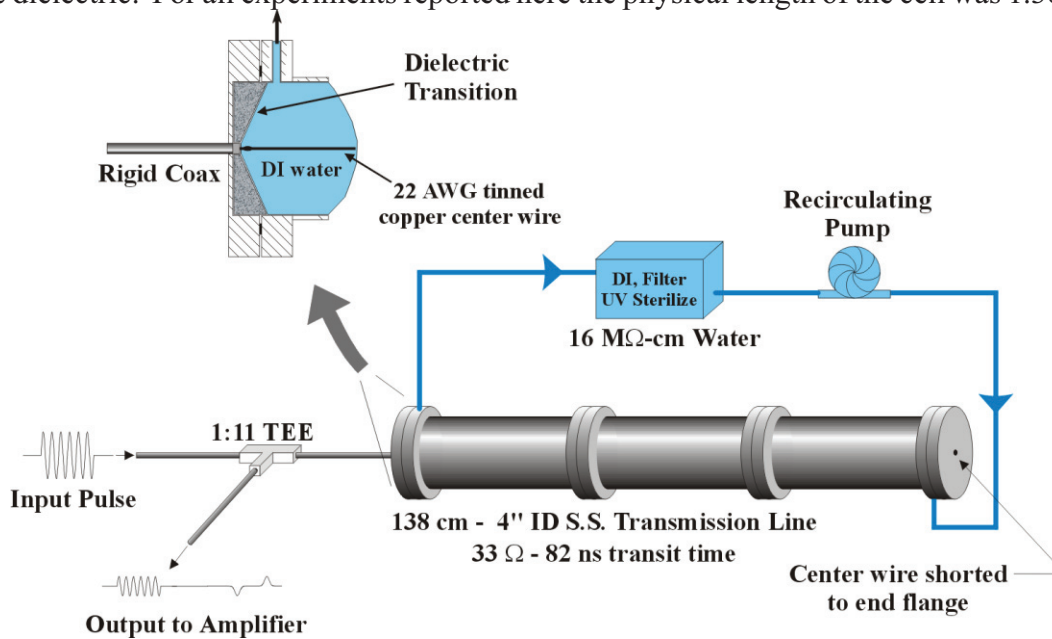
Figure 11 - Schematic diagram of the experimental setup for the coaxial water line. The inset detail shows the dielectric transition used to minimize problems with the reflection transient at the water line entrance.

The center conductor for the transmission line was tinned 22 AWG copper wire (0.66 mm diameter), shorted to the center of a blank flange at one end of the transmission line. The other end was soldered to the center conductor of a semi-rigid 50 Ω RG142 coaxial cable which was fed thru the center of another blank flange to introduce voltage pulses to the water line (see inset detail in Fig. 11). A dielectric (PVC), linearly tapered, microwave transition was placed at the RF-input side of the water line to reduce the perturbation that the RF signal experienced when launched into the water. The geometry of the transition was optimized by solving the steady-state Poisson's equation.

The coaxial water line was calculated to have a characteristic impedance of 33 Ω and a round trip transit time of 82 ns at 20 °C. Time-domain reflectometry (TDR) measurements verified these values to within 1% and showed that the input reflection transition had a duration of less than 1 ns. The measured reflection coefficient at the input interface was -20%.

Water was continuously circulated through the transmission line in a closed loop. As it recirculated

the water was deionized, mechanically filtered, and then biologically sterilized with an ultraviolet light source, resulting in nearly pure water with a resistivity of 16.5 MΩ-cm referenced to 25 °C. The test cell was not thermally stabilized, so the actual temperature of the water was determined by ambient conditions. During the course of an experiment the temperature of the water was typically measured to be 21 °C. For this reason the calculated waveforms shown below were obtained using the propagation parameters for water at 20 °C.

Fig. 11 also indicates the measurement method for these experiments. An input signal was sent into the test cell through a tap-off tee. The tap measured the input pulse and was monitored with an oscilloscope. The part of the signal that passed through the tee entered the water line, propagated down its length, reflected off the shorted end (inverting the pulse) and returned through the line again. The return signal emerged from the water line and was once again monitored by the tee. Thus the same oscilloscope trace captured both the input and output signals. The only difficulty for this method is that appropriate delay times must be chosen for the various signal cables to ensure that the pulses did not overlap.
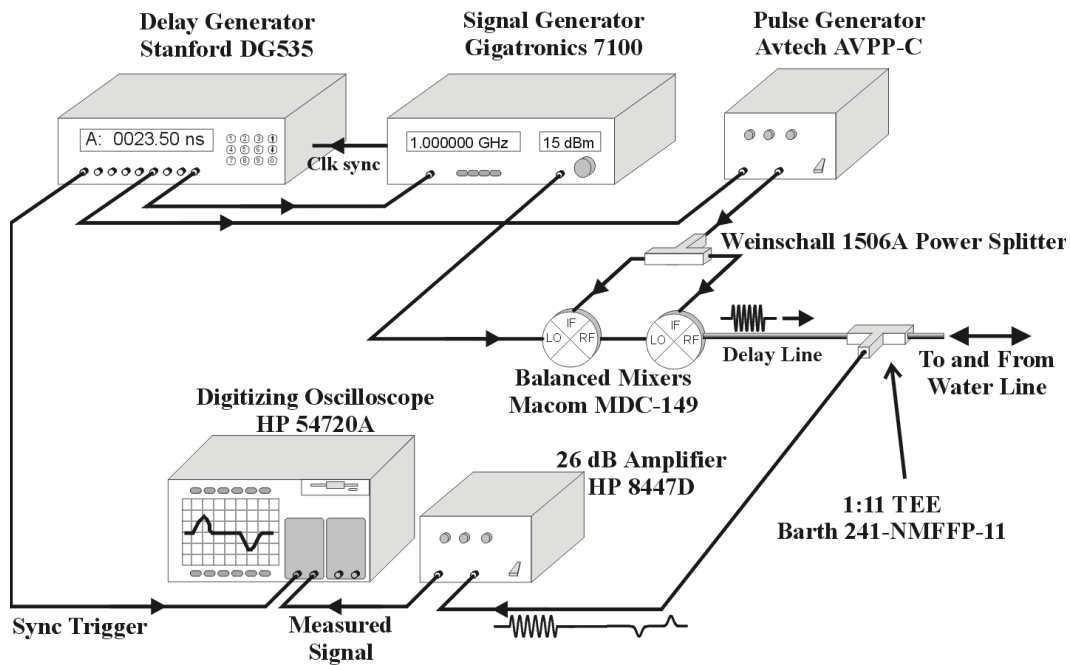
Figure 12 - Schematic diagram of the experimental arrangement used for the pulse generator and electrical diagnostics.

Fig. 12 shows a schematic diagram of the RF pulse generation system and electrical diagnostics for the experiment. A Stanford Research Systems DG535 delay generator and clock synchronized Gigatronics 7100 synthesized signal generator produced RF pulses with variable width but relatively slow risetime (≈2 ns). These pulses were used as the LO input for a serial pair of Macom MDC-149 mixers (RF/LO response 10-1500 MHz, IF response DC-1500 MHz). An Avtech AVPP-C pulse generator with <100 ps rise/fall time was triggered by the DG535 and used as the IF signal to modulate the slower pulses. Synchronization of the timing of the IF pulse with the RF phase of the Gigatronics 7100 was not sufficient to enable signal averaging, so for modulated-RF waveforms

each experimental measurement was made on a single-shot basis.

The RF pulse was sent down a foam core 50 Ω coaxial cable delay line (135 ns round trip) to a Barth 241-NMFFP-11 tap-off tee (DC-10 GHz pass thru and DC-5 GHz tap response). The pulse emerging from the tee was sent through 10 ft of RG142 semi-rigid coax (30 ns round trip) to the water line. These round trip times were chosen to prevent pulse reflections from overlapping the signals of interest.

The Barth tee tap responded to bi-directional signals on the main line, dividing the input signal by 11. Output from the tap was increased 26 dB with an HP8447D (0.1 to 1300 MHz) amplifier. Waveforms from the amplifier were recorded by an HP54720A digitizing oscilloscope, in conjunction with an HP54722A amplifier plug-in, which had an analog bandwidth (-3 dB) of >1.1 GHz and a digital sampling rate of 4 gigasamples/s (GS/s).

2.2.2 Square pulse results

The setup described above was used to make measurements of RF pulse propagation. To measure the propagation of a single square pulse the Avtech AVPP-C pulser was connected directly to the foam core delay line and the HP8447D amplifier was bypassed. Fig. 13 shows a typical raw oscilloscope trace for a fast-risetime 10 ns square pulse (note that this trace is similar to a TDR measurement of the experiment). The square pulse did not suffer the phase jitter problems mentioned previously, so this trace was averaged over 16 shots.
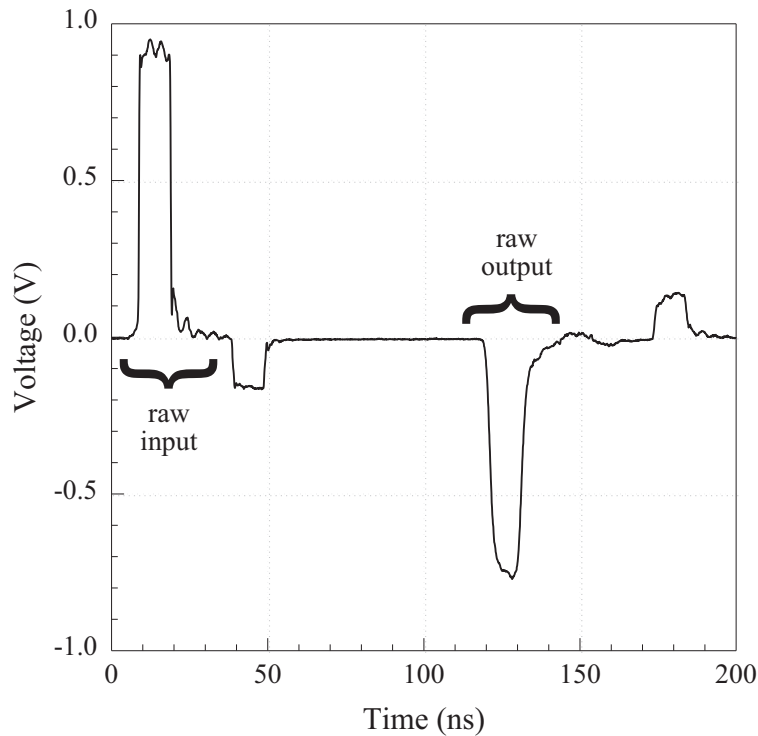
Figure 13 - Typical raw oscilloscope trace for a 10 ns square-pulse input to the water line. The labeled sections show the regions of interest for the measurements.

Several features of Fig. 13 should be noted:

27

- The section labeled "raw input" corresponds to the time window in which useful data about the input pulse could be collected.

- The raw input time is limited to about 30 ns by the inverted 20% return reflection from the water line.

- The section labeled "raw output" begins approximately 112 ns after the input pulse and corresponds to the signal propagated through the 2.76 meter round trip on the water line.

- The raw output time is limited to about 25 ns by the return of the reflection from the original input pulse off the Barth tee 135 ns after the original pulse is measured.

To process the measured results, the sections labeled raw input and raw output in Fig. 13 were extracted from the waveform file and treated independently. Each was scaled appropriately to account for the transmission and attenuation characteristics of the Barth tee, reflection and transmission at the entrance/exit of the water line, inversion due to the shorted water line, and the gain (when used) of the HP8447D amplifier.

Fig. 14 shows the results of processing the raw oscilloscope trace in Fig. 13. In Fig. 14a the pulse just after it enters the water line is seen to have an amplitude of about 7.5 volts and width of 10 ns. The plot with dashed line in Fig. 14b shows the measured return of this pulse after propagating 2.76 m as it appeared just before it exited the water line. As discussed in Sec. IId the return pulse exhibits slower risetime but little change in the pulse amplitude.

The dotted line in Fig. 14b is the expected return pulse as calculated with the FFT for water parameters at 20 °C using the trace in Fig. 14a as input. The only adjustable parameter in this and all subsequent comparisons between measured and calculated curves is a temporal translation of the calculated waveform to best fit the measured result. There is excellent quantitative and qualitative agreement between the calculated and measured traces, with less than 5 % error in the amplitude.

Fig. 14c shows the amplitude spectra for the 3 traces in Fig. 14a and 14b. The noise floor in our experiment is evident in the spectrum of the measured output at frequencies above 500 MHz. Averaging of the raw trace in this measurement provided signal to noise ratio of about 3 orders of magnitude. We see good agreement between the calculated and measured output spectra up to about 100 MHz. Between 100 and 400 MHz the general shape is the same, but the calculated spectrum is consistently greater than the measured. This explains why the measured return has a slightly slower risetime compared to the predicted response. Above 400 MHz the noise floor prevents any significant comparison.

It is difficult to calculate the error in these calculations due to the FFT approximation we are using because we do not have access to a closed form expression for the transform of the experimental signals. However, we note that in the ideal cases studied previously the bandwidths were only limited by the sampling interval we chose. Experimentally we have an analog bandwidth of about 1.1 GHz in the oscilloscope amplifier, which is far exceeded by the sampling rate of 4 GS/s. Therefore the replications of the spectrum at intervals of f_s which contribute to the error should not overlap appreciably.
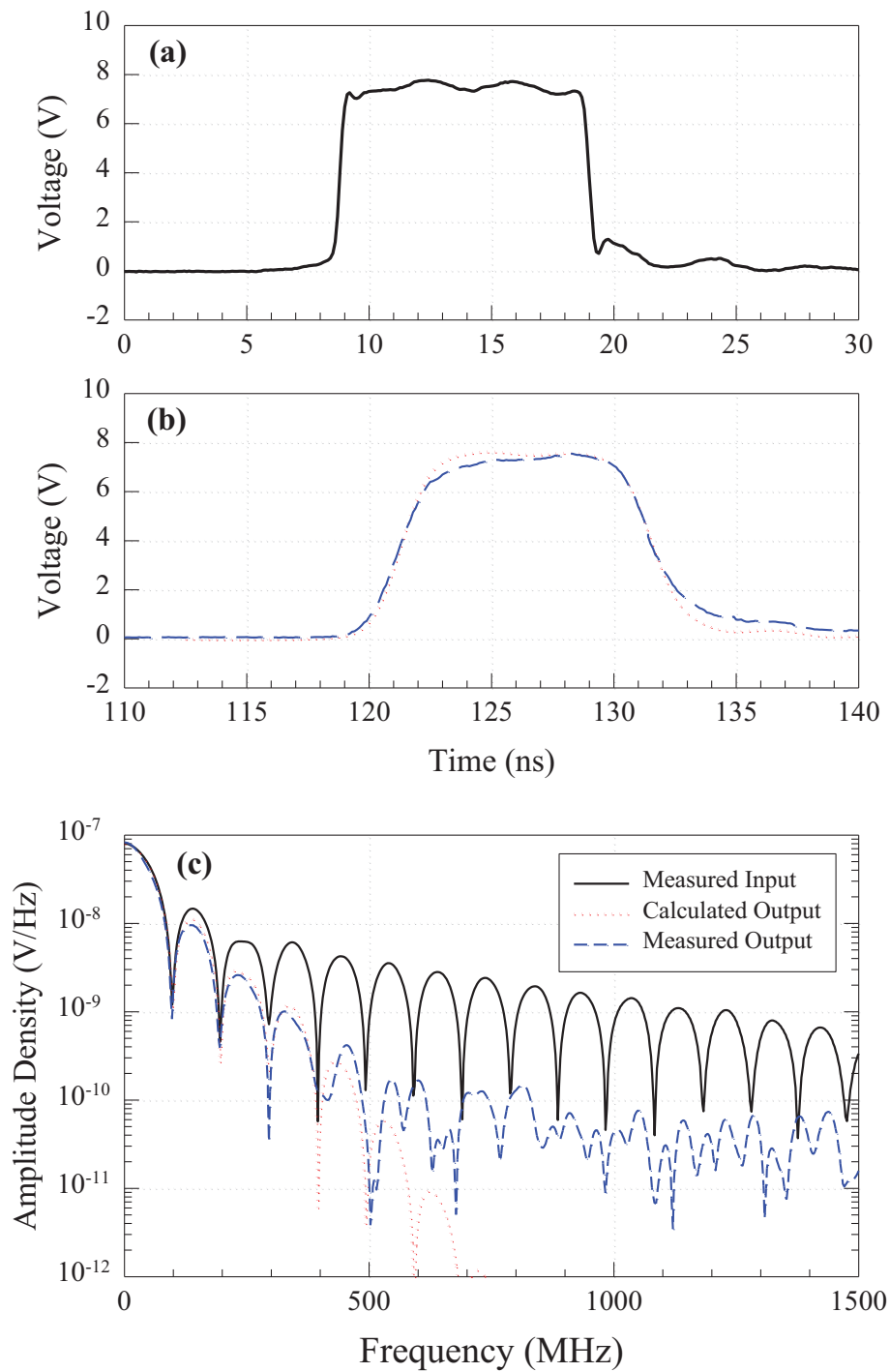
Figure 14 - Measured square-pulse propagation, derived from the raw trace in Fig. 12. (a) The voltage pulse just after it enters the water. (b) The measured and calculated return after the 2.76 meter round trip in the line. (c) Amplitude-density spectra for all three traces. The legend applies to all graphs.

2.2.3 Pulsed 1 GHz results

Fig. 15a shows a 10-cycle 1 GHz square-modulated pulse with an amplitude of about 60 mV at the start of the water line. The sampling interval of the digitizing oscilloscope (0.25 ns) is apparent in the coarse appearance of the trace. The return from this pulse in Fig. 15b shows the characteristic leading and trailing transients we expect. The qualitative similarity between Fig. 15b and Fig. 3c is very satisfying. The measured transient peaks are about 10% of the original pulse amplitude. Again, the predicted behavior of the pulse is well represented both qualitatively and quantitatively, with an error of about 15% at the peaks.

The spectra in Fig. 15c agree reasonably well out to about 300 MHz. There is some variation in the DC level, but this is not unreasonable given the possibility of superimposed noise and line variations in this experimental arrangement. There is more evidence of noise on the return pulse in this measurement for several reasons. The level of the return in the water line is about 5 mV, and this signal is measured while superimposed on whatever other noise, reflection, and source signals might be present on the extended transmission line. Additionally, the pulse is attenuated by a factor of 11 to sub-mV levels before being amplified by the HP8447D. Finally, the HP54720A amplifier has an RMS noise of about 300 µV.

Again we see the reason for the good agreement between measured and predicted time-domain waveforms in the spectra of Fig. 15c. The frequency components below 100 MHz are very well matched and they represent the primary contribution to the pulse characteristics. We also see that with a single shot measurement, the dynamic range decreased to about 2 orders of magnitude (roughly corresponding to the 8-bit digitization of the HP54720).

Evident in the pulse of Fig. 15 and all other experimentally observed RF waveforms, the polarity of the transients was determined by the polarity of the first and last half-cycle of the input voltage pulse. This is further demonstrated by the results in Fig. 16. A 10.5 cycle 1 GHz pulse with amplitude of about 50 mV is shown in Fig. 16a, with the corresponding measured return in Fig. 16b. The first and last half-cycles of the input pulse are positive, which in turn produces two positive transients at the output. This result provides strong experimental validation for the method and assumptions we use to treat the DC component.

We present no graphical data for the case of trapezoidal modulation at 1 GHz because it was a null result for these experimental conditions. When the risetime of the input pulse was degraded in any way at 1 GHz there was no measurable transient pulse. Further, the phase jitter in our experiment and pulse-width jitter from the Avtech pulse generator meant there was significant shot to shot variation in the RF pulse waveform. If the modulation pulse turned on at some intermediate point in an RF cycle, it was equivalent to a slow rise or fall time and no transients were generated. The pulsewidth variation meant that sometimes the modulation would turn on mid-cycle, but turn off at the end of a complete cycle, or vice-versa. In that case we often saw only a leading or trailing individual transient corresponding to the sharp-edged transition. This behavior was consistent with calculations from ideal waveforms with asymmetric trapezoidal modulation.
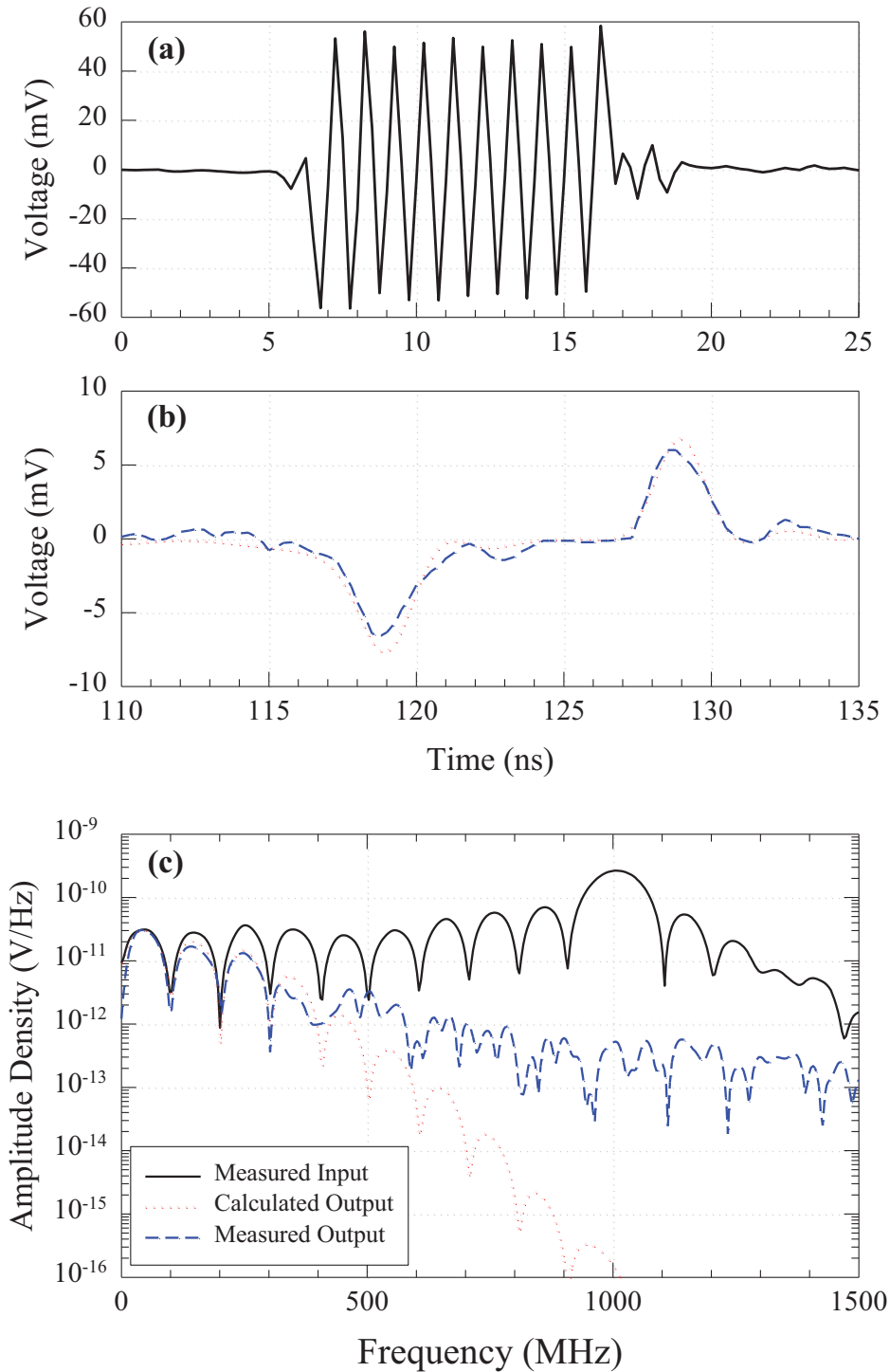
Figure 15 - Measured propagation of 1 GHz, 10-cycle square-modulated voltage pulse. (a) The
pulse after it enters the water. (b) The measured and calculated return pulse after the
2.76 meter round trip through the water line. (c) Amplitude-density spectra for all
three traces. The legend applies to all graphs.
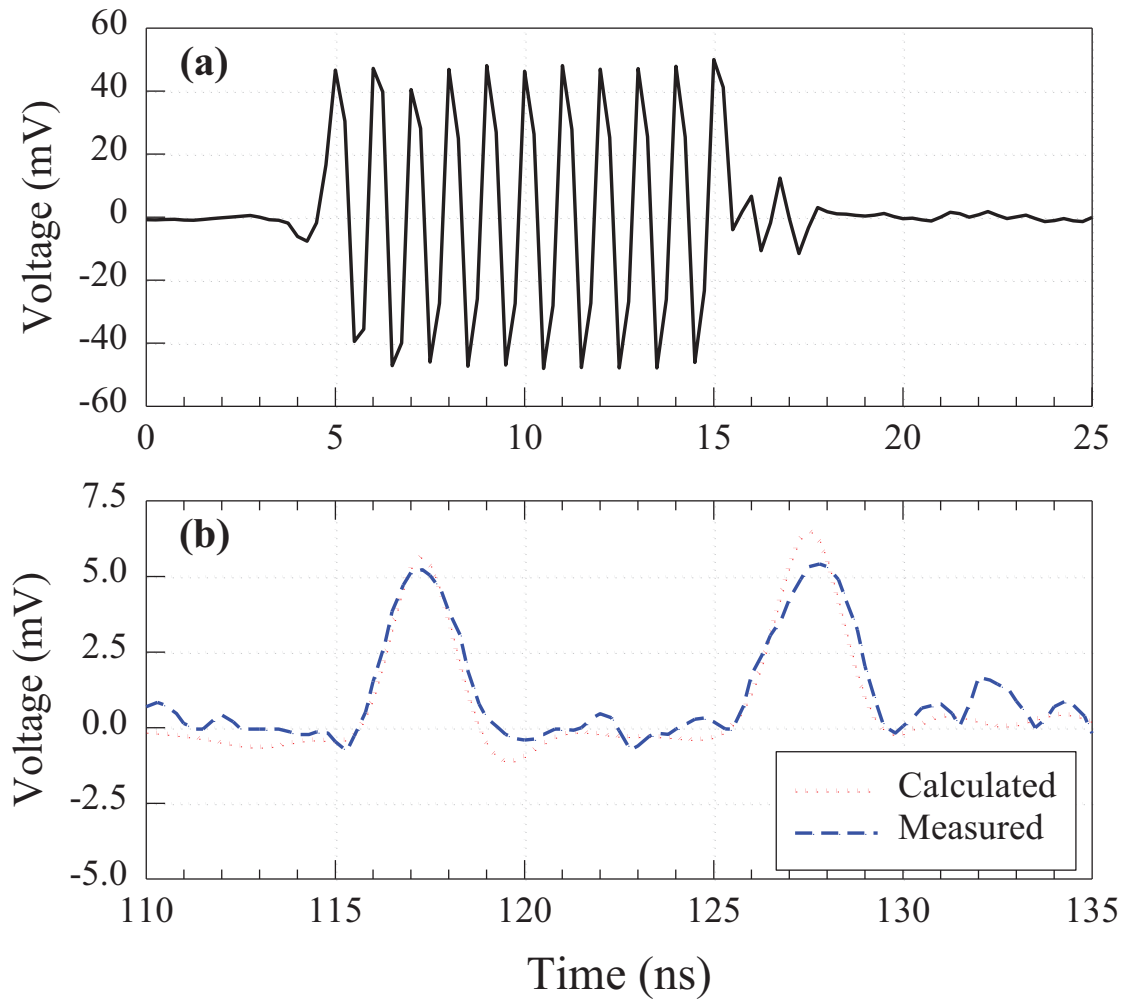
Figure 16 - Measured propagation of 1 GHz, 10.5 cycle square-modulated voltage pulse. (a)
The pulse after it enters the water. (b) The measured and calculated return pulse
after the 2.76 meter round trip through the water line.

2.2.4 Pulsed 400 MHz results

For the fixed 2.76 meter propagation length of our experiment there was no measurable 1 GHz
component in the return pulse. Changing the RF carrier to a lower frequency made it possible to
observe both the leading and trailing transients as well as the lower amplitude remnant carrier. Fig.
17 shows experimental results for a 6-cycle 400 MHz square-modulated pulse. In Fig. 17b the
measured return pulse has the lower frequency leading/trailing transients we expect, as well as a
remnant of the 400 MHz fundamental.   For this particular measurement the transient peak
amplitudes were two to three times that of the fundamental. Fig. 18 shows results for a 5.5 cycle 400
MHz pulse similar in character to Fig. 16.   Again we see the transient polarity dictated by the
polarity of the first and last half cycles of the pulses.
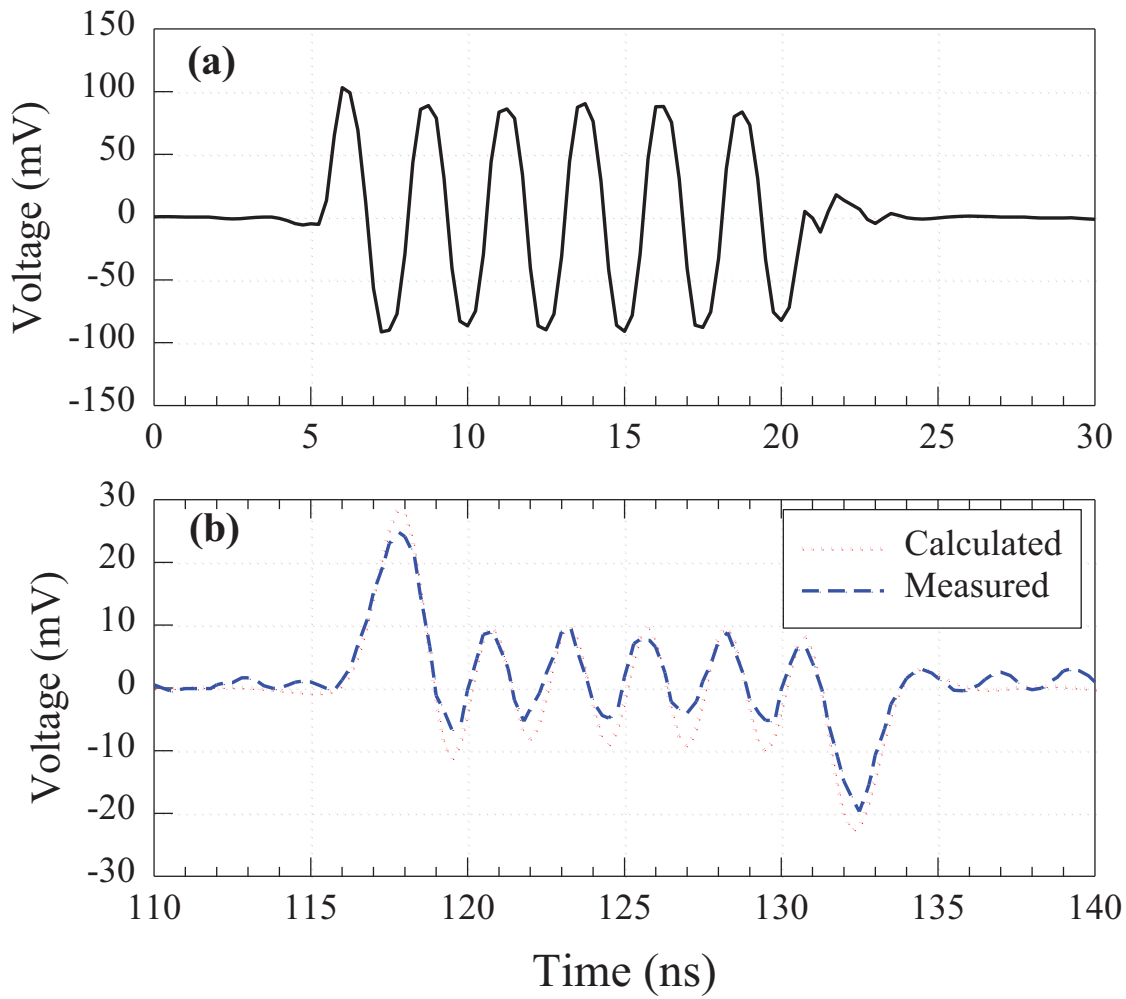
Figure 17 - Measured propagation of 400 MHz, 6-cycle square-modulated voltage pulse. (a) The pulse after it enters the water. (b) The measured and calculated return pulse after the 2.76 meter round trip through the water line.
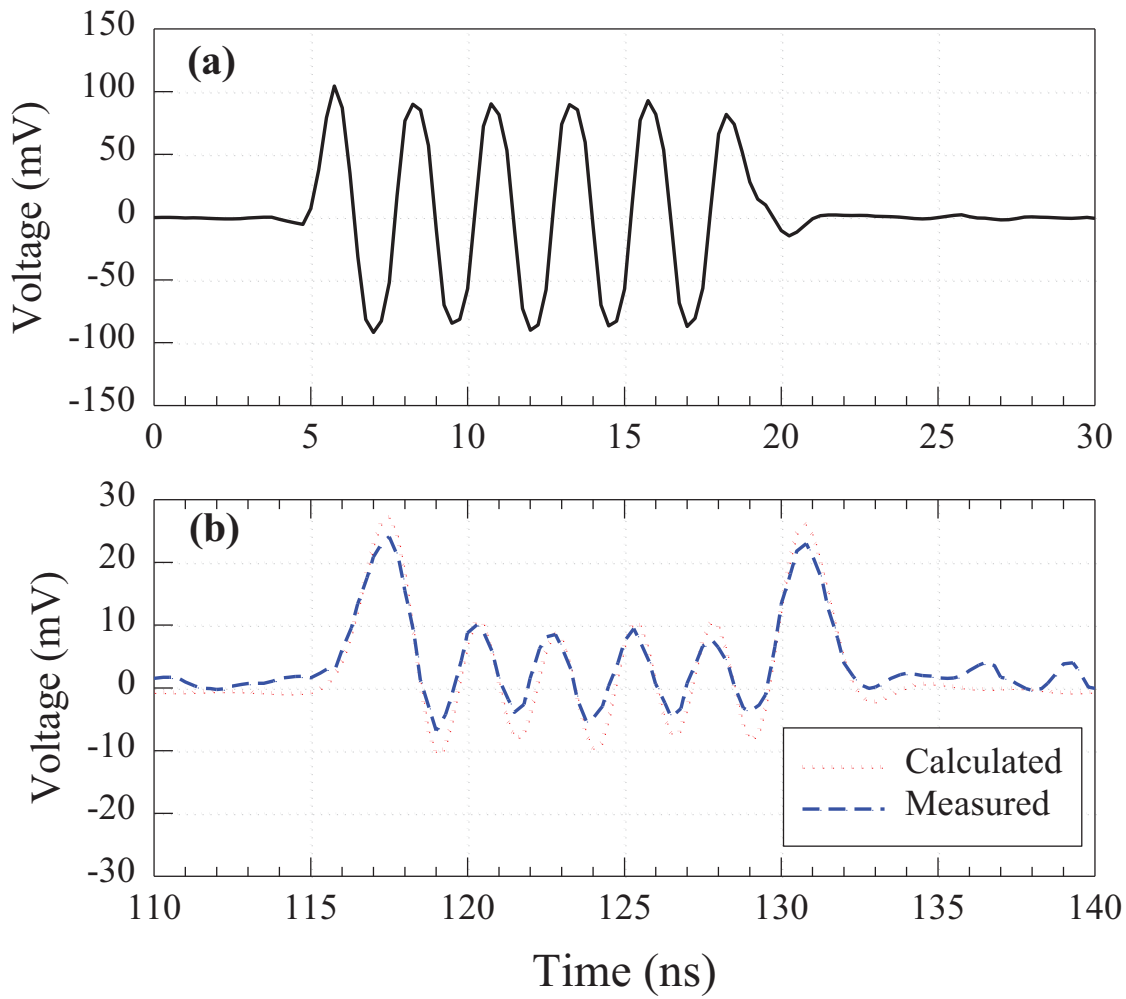
Figure 18 - Measured propagation of 400 MHz, 5.5-cycle square modulated voltage pulse. (a) The pulse after it enters the water. (b) The measured and calculated return pulse after the 2.76 meter round trip through the water line.

Using a slow-risetime pulse from the Stanford DG535 to directly modulate the mixers (bypassing the Avtech AVPP-C) we were able to produce symmetric trapezoidal modulation at 400 MHz with rise and fall time of about 2 ns. Fig. 19 shows the results for a 6-cycle pulse. The measured output in Fig. 19b shows no evidence of the leading and trailing transients. If anything, the third half-cycle peak is emphasized. The general behavior and amplitude for this case is consistent with both the calculated result for the experimental input, and with the form displayed by the ideal case in Fig. 7.
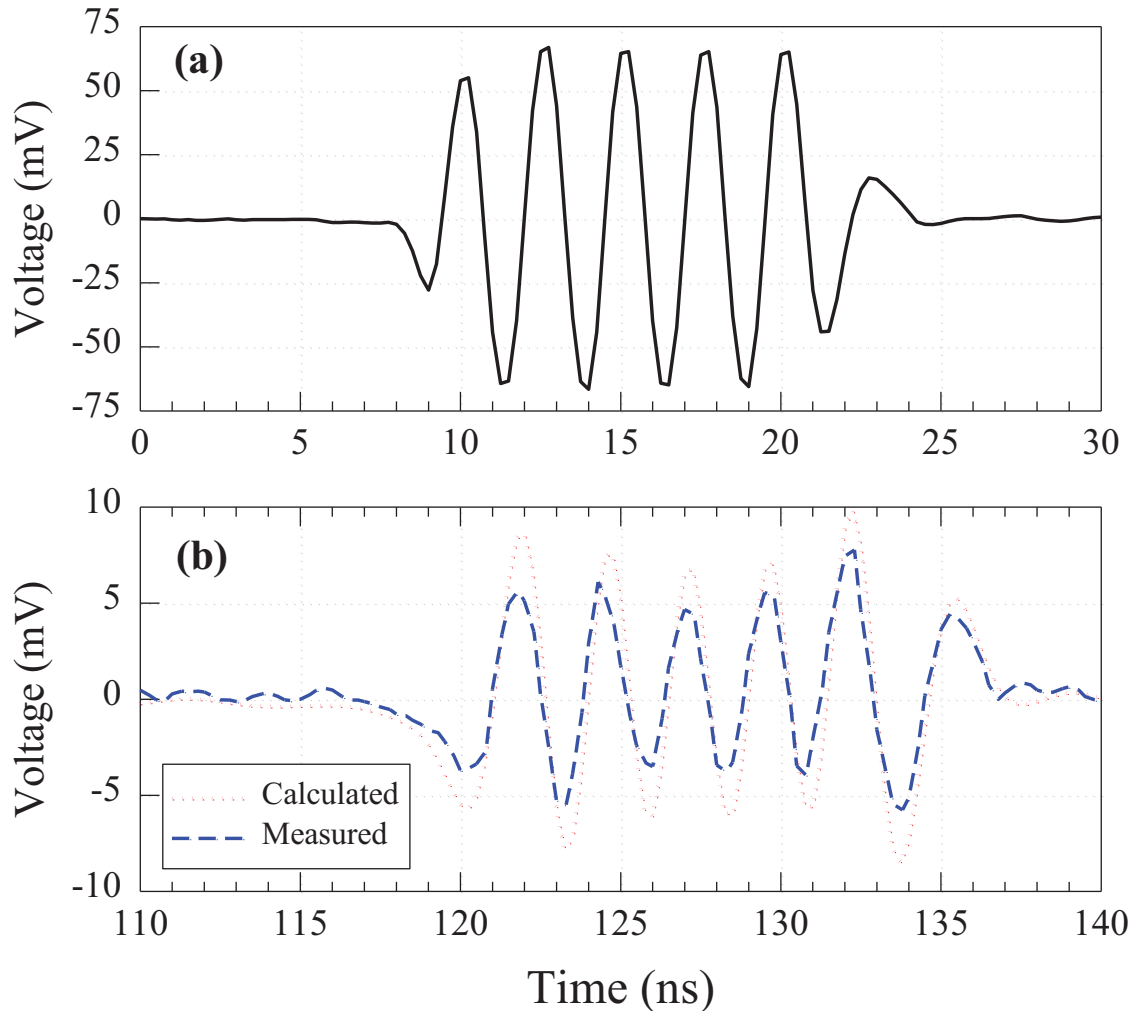
Figure 19 - Measured propagation of 400 MHz, 6-cycle trapezoidal-modulated voltage pulse with ≈2.5 ns rise and fall time. (a) The pulse after it enters the water. (b) The measured and calculated return pulse after the 2.76 meter round trip through the water line.

2.2.5 Offset RF burst

We could generate an offset RF-modulated square pulse using the arrangement described in Fig. 12 by disconnecting the IF input to the second Macom mixer. However, the quality of the pulse was very much a function of the carrier frequency and was suitable for measurement only in a narrow

frequency range around 800 MHz.

Fig. 20 shows experimental results for an offset RF burst consisting of 10 cycles at 800 MHz. The input pulse in Fig. 20a has an amplitude of about 10 mV. The measured return in Fig. 20b is qualitatively very similar to the return from the square pulse in Fig. 14b. No evidence of the 800 MHz modulation survives, as predicted in the discussion of Sec. IIe. Fig. 14b also shows excellent calculated agreement with the measured return, with an average amplitude error of <10%.
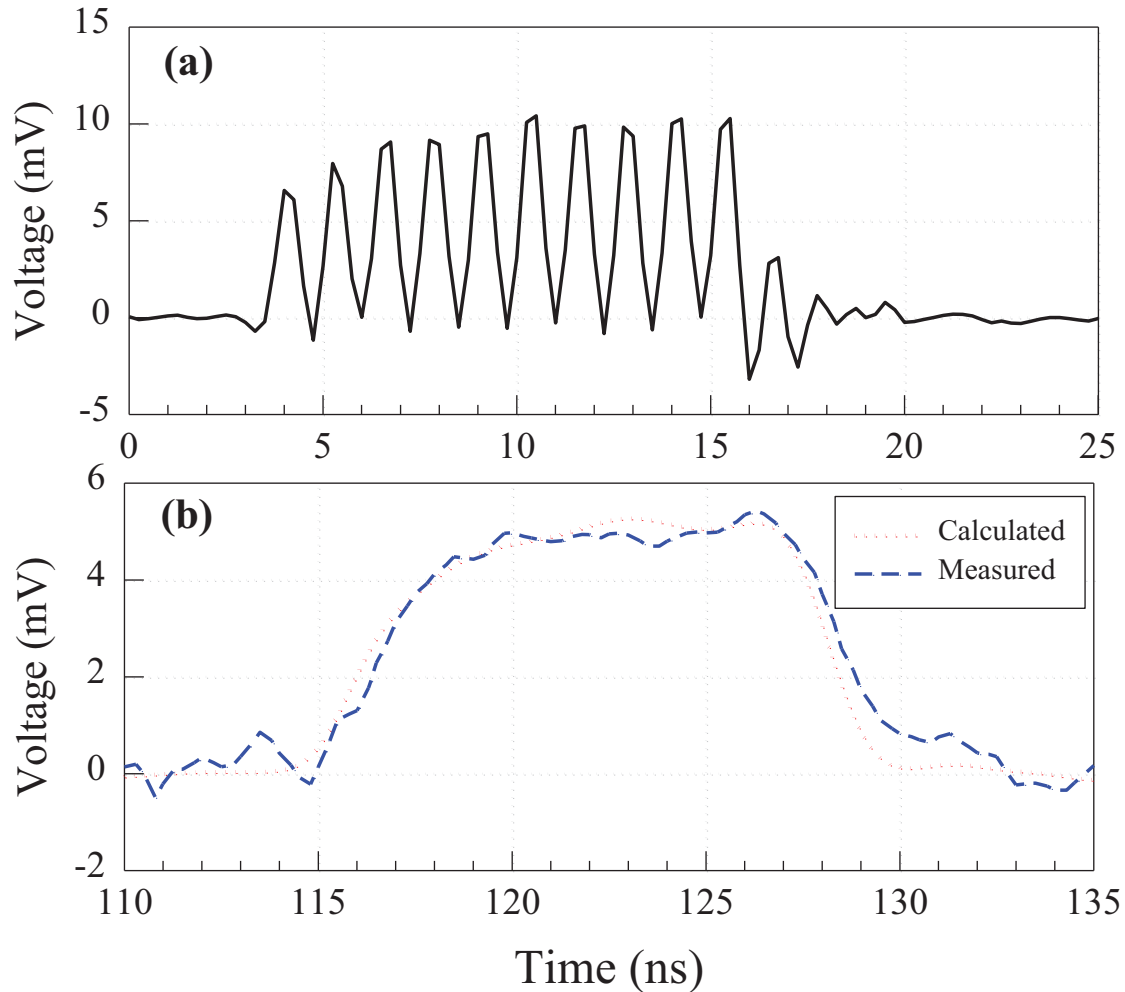
Figure 20 - Measured propagation of 800 MHz, 10-cycle offset voltage pulse. (a) The pulse after it enters the water. (b) The measured and calculated return pulse after the 2.76 meter round trip through the water line.

2.3 Discussion

We have examined the transient fields related to the leading and trailing edges of square-wave modulated RF and microwave pulses propagating in deionized water both numerically and experimentally. We found excellent experimental agreement with the qualitative predictions of pulse distortion and the quantitative values of the transient peaks. The strong frequency dependence of the attenuation coefficient of deionized water over the frequency range we investigated leads to

non-uniform attenuation of the spectral components contained in the RF pulse. The non-uniform attenuation increases the relative contribution of the low-frequency part of the pulse spectrum. The transient fields were shown to be simply the result of the low-frequency harmonic content contained in the initial pulse.

The transients we have been examining are very much related to Brillouin precursors in that they derive from the low frequency portion of the pulse spectrum. Brillouin precursors have been shown to result from the leading and trailing edges of a sharply-modulated sinusoidal field at optical frequencies propagating in a medium exhibiting anomalous dispersion. In fact, the transients shown in Fig. 3 are qualitatively very similar to those shown in Fig. 20 of Ref. [19], in which a square-wave-modulated optical pulse, with a width of 5.026×10^{-15} sec, corresponding to eight cycles of UV radiation, propagated in a strongly dispersive and absorptive Lorentz medium.

The material that has been used for the investigation of precursor phenomena has primarily been a dielectric Lorentz medium with a single-resonance frequency. This type of medium is locally linear, homogeneous, isotropic, and causally dispersive [21]. In the frequency range we are considering, however, water does not exhibit anomalous dispersion (see Fig. 1). The important difference between the results in Ref. [19], and those shown here and in Ref. [3], is that the propagation velocity of the microwave transients in water is the same as the propagation velocity of the fundamental at 1 GHz. In Ref. [19] the propagation velocity of the Sommerfeld precursor fields are equal to the propagation velocity of light in a vacuum, and the propagation velocity of the Brillouin precursor fields are also slightly higher than the velocity of the carrier frequency in the medium. The main reason why the pulse distortion that occurs in water below 2 GHz is similar to that shown in Ref. [19] is because the rapid rise in the absorption coefficient, shown in Fig. 1b, resembles the rapid increase in the absorption coefficient of a Lorentz medium exhibiting anomalous dispersion. In other words, the region over which anomalous dispersion occurs is also the frequency interval where resonant absorption occurs.

Because of the similarities noted above, several authors have chosen to identify these leading and trailing microwave transients as Brillouin precursors. Although it is perhaps only a matter of semantics, we choose not to do so because of the confusion this term introduces. Sommerfeld and Brillouin originally were interested in understanding the ramifications of varying phase, group, signal, and energy velocities for a pulse with a center frequency in a region of anomalous dispersion. The terms "precursor" and "forerunner" derive from the fact that the high and low frequency components of the signal travel faster than the center frequency and thus arrive earlier. For water below 2 GHz there is no difference in propagation speed, the low frequency components do not travel faster than the center frequency of the pulse, and there is nothing "pre" about the transient which develops. It results solely from frequency dependent absorption.

As shown in Fig. 4, the transient peak fields decay approximately as $1/z^{1/2}$ over the interval 1 to 10 meters. This fact could have significant impact on the determination of the biological effects of modulated microwave fields. However, it has also been proposed that RF waveforms that result in these transient fields may be especially hazardous to humans [22]. At this point, there appears to be little evidence that demonstrates that these transient fields are any more harmful than lower-frequency square-wave modulated RF pulses. As a result of the lower frequency content, these pulses would also penetrate more deeply into biological media.

CHAPTER 3 - Propagation in Saline Water

3.1 Objectives and Approach

The objective of this work was a comprehensive analysis of the evolution of a modulated microwave pulse in saline water that builds up the results for deionized (DI) or pure water. The analysis included theoretical predictions, but tailored the model for direct experimental verification. The investigative approach is straightforward. First, the water dielectric response as a function of frequency is defined using the Debye model. The parameters in this model are further defined in terms of the experimentally controllable variables of salinity (the ratio of the salt to water mass) and the water temperature. The modeled dielectric response is then used to characterize the dielectric medium of a water transmission line. Using this derived transfer function, several input signals are defined and returns predicted for a range of water salinity.

In addition to the study of the basic propagation of signals in water, the results from the model of the transmission line were used to determine both reasonable physical dimensions of the experimental setup and to predict the magnitude of the output signal given a specific pulse amplitude and shape. Based on the results calculated for several transmission line geometries, an experimental structure with similar dimensions was designed and a pulse generating circuit assembled. The output signal for a standard input was then experimentally measured for several different values of salinity. These measured waves were compared with the theoretically predicted values to confirm the validity of modeling.

The relatively high conductivity of the saline water results in high loss when compared to the pure water case, especially at lower frequencies. As will be described below, this required the project to be expanded beyond the original pure water study in two ways. First, the theoretical analysis had to be amended to include the full phase description of the wave propagation. In fresh water the propagation could be modeled with a purely real, frequency dependent loss factor. This approximation is not valid for water with salinity. Second, the voltage level of the experimentally measured signal was significantly lower. To measure the lower signal, a transmission line and pulse generator were built and the pulse format changed, based on results of the pure water study. This allowed the use of data averaging to increase the signal to noise ratio.

3.2 Numerical Analysis

3.2.1 Complex dielectric response of water

The electrical response of water can be approximated by the Debye dielectric model. This approximation defines the response as a function of both frequency and material parameters by describing the behavior of the water molecule as a dipole with a thermal restoring force.[23] By this model, the complex form of the relative dielectric response is given by the equation

$$\widetilde{\varepsilon} = \varepsilon_\infty + \frac{\varepsilon_{DC} - \varepsilon_\infty}{1 - i2\pi\tau f} + i\frac{\sigma_{DC}}{2\pi\varepsilon_0 f} \tag{14}$$

where ε_∞ and ε_{DC} are the high frequency and static dielectric constants respectively, ε_0 is the

permittivity of free space, σ_{DC} is the low frequency conductivity, and τ is the molecular relaxation time. Typical values for water at room temperature are $\varepsilon_\infty \sim 4.9$, $\varepsilon_{DC} \sim 80$, and $\tau \sim 8.6 \times 10^{-12}$ sec. These physical parameters have been measured by others and depend on salinity and water temperature.[24]

Referring to the Debye model equation, the direct current conductivity, σ_{DC}, approaches zero for DI water. This forces the third term on the right hand side of the equation to go to zero for all finite frequencies. Therefore in DI water, the frequency dependence is described by the second term of the equation. At low frequencies, where $2\pi\tau f << 1$, the imaginary part of the denominator is insignificant. Therefore for these low frequencies, the dielectric response is nearly real and not dispersive. As the frequency increases the imaginary component, or equivalently the absorption in the water, abruptly increases.

As was shown previously, the water in this way acts very much like a depth-dependent low-pass filter, absorbing most of the high frequency content of the input pulse. After propagating only a few meters nearly all of the high frequency energy is absorbed and the low frequencies remain unchanged. This was the basis for the modeling of microwave pulses in DI water. Since, the frequencies that undergo significant dispersion are also greatly attenuated, the evolution of the wave packet can be evaluated by simply applying frequency dependent absorption. There is not sufficient space here to thoroughly report the results, however the validity of the approximation for zero salinity water was confirmed by a comparison of the expected pulse shape using this approximation to the predicted shape using a calculation based on a full complex form. No discernable difference in the expected output was found even when the assumed path length for the simulation was tens of meters through DI water.

Although a model employing only absorption is sufficient for the DI water analysis, as salinity increases and σ_{DC} increases, the contribution of the third term in Equation 14 becomes important. The frequency dependent absorption described above for the fresh water is still significant, however higher conductivity results in more loss at low frequencies. By the constraint of causality, increasing absorption means greater phase dispersion. This dispersion results in a complicated evolution of the pulse envelope since each frequency propagates at a different velocity. This requires defining a transfer function using a full complex form of the Debye model as in Equation 14 and therefore, was the basis for the saline water analysis.

The Debye model describes the effect of saline water on the development of an electromagnetic wave. In order to relate the theoretical results to measurements that can be obtained in the laboratory, the water transfer function was used to define the dielectric of a bounded transmission line. The model of the transmission line not only accounts for the absorption in the saline water but also the dispersive reflection and transmission coefficients at the input and output of the line.

3.2.2 Definition of the input pulse.

A primary goal of the study was to measure the evolution of fast transient microwave pulses as they propagate through saline water. In the pure water study, the pulses used for measuring the effects of the DI water were square modulated microwave pulses, 10 to 20 ns of duration, with a center frequency between 100 kHz and 1 GHz. These pulses were generated by mixing a constant center frequency signal with a fast transient gate pulse. Although the technique resulted

in a useful modulated waveform, the peak amplitude was limited by the available signal
generator. Also, the phase of the modulation jittered from shot to shot, preventing averaging of
the measured output. Because of the increased absorption with salinity, these limitations led to
the conclusion that a different input waveform was needed for this study than those used for
deionized water. The new pulse consists of a complimentary pair, one positive going and one
negative going, of fast risetime pulses separated by the same duration as the window of the
original waveform, 10 to 20 ns. The pulses were generated by passing a sub-nanosecond
risetime square pulse through a fast differentiator. This new pulse is very similar in amplitude
and phase at low frequency when compared to a typical waveform in the pure water study.
Recall from the conclusions of that work, the low frequency characteristics of a modulated pulse
are defined by the transients of the modulation envelope and generally maintain their amplitude
and phase during pure water propagation. Therefore the low frequencies contain most of the
energy that transits any substantial distance in the pure water. The differentiated pulse does not
contain as much high frequency energy (100 kHz – 1 GHz) as that found in the modulated
microwave pulse but is very similar in overall content to a modulated pulse that has propagated
in pure water. Since the same mechanisms are still present in the saline water, the differentiated
input pulse without the modulation should give essentially the same information about the
evolution of the dominant components of the pulse spectrum, while being a more practical and
efficient test pulse for experimental validation.
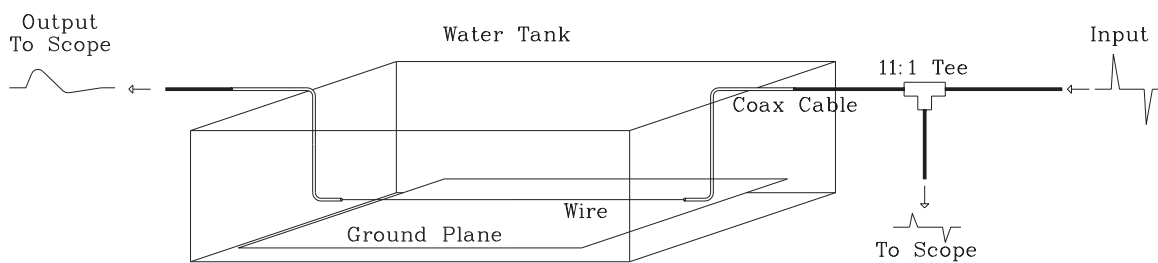
Figure 21 - Schematic of water transmission line. The coax line enters the water tank, transitions
to a monofilar line, back to a coax line, and feeds directly to the oscilloscope.

3.3 Experimental Measurements.

The water transmission line is shown schematically in Figure 21. The input pulse is generated
using an Avtech AVPP-1 pulse generator feeding a differentiating filter. The coaxial filter has a
sub-nanosecond risetime and approximately a 3 ns time constant. A 10dB attenuator was placed
in the line before the filter to damp out reflections between the filter and the source. The
differentiated pulse is fed from the filter into approximately 8 m of 50 ohm Heliax transmission
line to a Barth – 241, 11:1 signal splitter. The splitter has a tap-off that provides an attenuated
version of the passing input signal. This tap-off signal was monitored on channel A of a Hewlett
Packard 54720-A oscilloscope. From the splitter, the primary pulse proceeds along
approximately 3 m of rigid coax to the water line input transition. This coax delay line provides
time isolation of the wave reflected from the transmission line for the duration of the input pulse.
The transition feeds the coaxial wave into the 30 cm long monofilar line, (a single conductor
above a ground plane). A complimentary transition is then made on the output of the line to
another length of coax and finally to the second channel of the scope.

The theoretical modeling was used to set the water line design criteria. An important result of the model analysis was an estimation of the expected output return for a given water line length and saline concentration. The output waveforms, even for modest saline concentrations, were predicted to have amplitudes several orders of magnitude lower than the signals measured in DI water. The line propagation length was chosen to be short enough to maintain measurable signal levels, but long enough to allow a significant dispersion during the pulse propagation. Since the line was significantly shortened from that used for the previous DI experiments, it was also built with much smaller dimensions. The new monofilar configuration was chosen to maximize the impedance while minimizing the line dimensions. The line is constructed of .24 mm diameter stainless steel wire stretched 8 mm above a thin stainless steel sheet. The ground transitions from the coaxial line to the monofilar geometry were roughly "zippered" in an attempt to minimize frequency dependent losses due to the change in geometry of the system. The line and ground plane sheet were mounted on a plastic base and immersed in a water tank. The water in the tank was circulated by a pump and filtered with a fine particulate inline filter. The water temperature and salinity were monitored with an electronic thermometer and a salinity probe.

Examples of measured and calculated data for three different salt concentrations are shown in Figure 22. The propagation distance in water is the length of the monofilar line, which is approximately 30 cm. The input waveform for each of the data sets was a differentiated pulse, with a positive to negative peak time delay of 10 ns. For the numerical data, the input for the calculation is the measured input for the corresponding experimental waveform. This time domain data was Fourier transformed to the frequency domain, multiplied by the appropriate transfer function, and inverse transformed back to the time domain.

The shape of the input wave is evident in the salinity (S)=.3 data. Although the water filtered some of the very high frequency content resulting in a slightly longer risetime, the basic form of the input wave is intact. The similarity of this pulse to the DI water data reported in the pure water study for a modulated pulse propagating through 3 m of water is strikingly apparent (See Fig. 15 in Chapter 2). This reinforces the supposition that the differentiated pulse can be used as the generic input wave to study the propagation of a modulated pulse.

3.4 Discussion.

Comparing these data, they demonstrate several important details about the propagation of microwave pulses in saline water. First, the peak amplitude of the signal is falling superlinearly with increasing salinity. This is a result of the linear increase in the exponential absorption coefficient as the conductivity increases. Also, note that although the loss of the high frequency content clearly increases the risetime, it is the fall time of the pulse that shows the most notable increase. This results in a dramatic time lengthening of the output pulse, as is apparent by comparing the ordinate scales corresponding to each salinity. As the salinity is increased, each pulse is broadened until, as seen for $S = 10$, the input pulse width of 10 ns simply defines the location of the critical maximum of the signal. Note that although each of the waves have long trailing tails, the leading edge is relatively well defined as would be expected for a signal propagating in a real causal medium. This temporal asymmetry on the output return from an effectively symmetric input is a direct consequence of the phase dispersion introduced by the saline water.
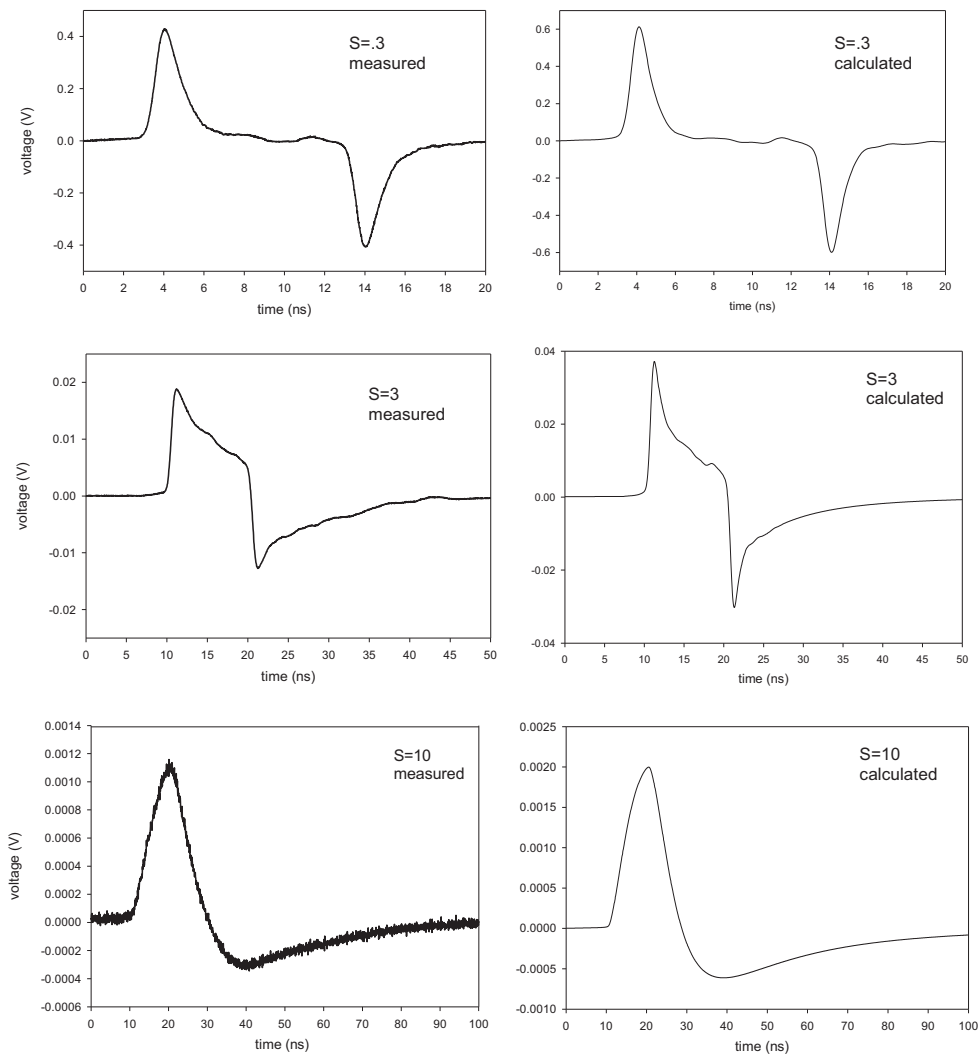
Figure 22 - Measured and calculated output waveforms from the monofilar line for three saline concentrations.

Comparisons between the predicted and measured waveforms show notable differences in pulse amplitude, especially at the elevated salinity levels. Although these differences do not follow a simple linear scaling factor as would be expected for errors introduced because of tolerances in experimental setup (such as the transmission line dimensions), the good agreement in the temporal behavior indicates that the dielectric response is being modeled adequately. The difference is probably due to point losses at the water line input and output transmissions or from variations in the dimensions of the line along its length. Even with the amplitude differences, the temporal behavior of the pulse is well represented by the model and shows the utility of the modeling approach.

REFERENCES

1.   C.H. Durney, "Electromagnetic dosimetry for models of humans and animals: A review of theoretical and numerical techniques," *Proc. IEEE*, Vol. 68, pp. 33-40, 1980.

2.   S.M. Michaelson, "Microwave biological effects: An overview," *Proc. IEEE*, Vol. 68, pp. 40-47, 1980.

3.   R. Albanese, J. Penn, and R. Medina, "Short-rise-time microwave pulse propagation through dispersive biological media," *J. Opt. Soc. Am. A*, Vol. 6, pp. 1441-1446, 1989.

4.   K. Moten, C.H. Durney, and T.G. Stockham, Jr., "Electromagnetic pulse propagation in dispersive planar dielectrics," *Bioelectromagnetics*, Vol. 10, pp. 35-49, 1989.

5.   F.X. Hart, "Pulse shape distortion by tissues," *J. Bioelectricity*, Vol. 6, pp. 93-107, 1987.

6.   J.C. Lin and C.K. Lam, "Coupling of Gaussian electromagnetic pulses into a muscle-bone model of biological structure," *J. Microwave Power*, Vol. 11, pp. 67-75, 1976.

7.   T.M. Roberts and P.G. Petropoulos, *Asymptotics and energy estimates for electromagnetic pulses in dispersive media*, Southern Methodist University Math Report 95-6.

8.   A. Sommerfeld, *Ann. Phys*,. Vol 44, pp. 177-202, 1914. L. Brillouin, *Ann. Physik*., Vol. 44, pp. 203-240, 1914. For English translations see, L. Brillouin, *Wave Propagation and Group Velocity*, New York: Academic Press, 1960.

9.   K.E. Oughstun and G.C. Sherman, *Electromagnetic Pulse Propagation in Causal Dielectrics*, New York: Springer Verlag, 1994.

10. J. Aaviksoo, J. Kuhl, and K. Ploog, "Observation of optical precursors at pulse propagation in GaAs," *Phys. Rev. A*, Vol. 44, 5353, 1991.

11. P. Pleshko and I. Palócz, "Experimental observation of Sommerfeld and Brillouin precursors in the microwave domain ", *Phys. Rev. Letters*, Vol. 22, 1201, 1969.

12. J.G. Blaschak and J. Franzen, "Precursor propagation in dispersive media from short-rise-time pulses at oblique incidence," *J. Opt. Soc. Am. A*, Vol 12, 1501-1512, 1995.

13. K.E. Oughstun, J.E.K. Laurens, C.M. Balictsis, "Asymptotic description of electromagnetic pulse propagation in linear dispersive medium," *Ultra-Wideband, Short-Pulse Electromagnetics*, H. Bertoni, ed., Plenum Press, 1993, 223-240.

14. R.R. Smith, *Dispersive pulse propagation*, Defense Nuclear Agency technical report #DNA-TR-88-262, 1988.

15. E.H. Grant, R.J. Sheppard, and G.P. South, *Dielectric Behaviour of Biological Molecules in Solution*, Oxford: Clarendon Press, 1978. Also, personal communication between E.H. Grant, King's College, University of London, and J.W. Penn, School of Aerospace

Medicine, Brooks Air Force Base, 1988.

16.   J.D. Jackson, *Classical Electrodynamics, 2nd Ed.*, New York: Wiley & Sons, 1975.

17.   C.D. McGillem and G.R. Cooper, *Continuous and discrete signal and system analysis, 2nd ed.*, New York: Holt, Rinehart and Winston, 1984.

18.   R.K. Adair, *"*Ultrashort microwave signals: a didactic discussion," *Aviat. Space and Environ. Med.*, Vol. 66, pp. 792-794, Aug. 1995.

19.   K.E. Oughstun and G.C. Sherman, *"*Uniform asymptotic description of ultrashort rectangular optical pulse propagation in a linear, causally dispersive medium," *Phys. Rev. A*, vol. 41, 6090-6113, 1990.

20.   V. Mac Clean, R. Sheppard, and E. Grant, "A generalized model for the interaction of microwave radiation with bound water in biological material," *J. Microwave Power*, Vol. 16, pp. 1-7, 1981.

21.   H.M. Nussenzveig, *Causality and Dispersion Relations*, New York: Academic Press, Chap. 1, 1972.

22.   R. Albanese, J. Blaschak, R. Medina, and J. Penn, "Ultrashort Electromagnetic Signals: Biophysical Questions, Safety Issues, and Medical Opportunities," *Aviat. Space and Environ. Med.*, pp. A116-A120, May 1994.

23.   J. Lane and J. Saxon, "Dielectric dispersion in pure polar liquids at very high frequencies. III. The effect of electrolytes in solution," *Proc. Roy. Soc.*, vol. A213, 1952, pp. 531-45.

24.   A. Stogryn, "Equations for Calculating the Dielectric Constant of Saline Water," *IEEE Trans. Microwave Theory and Tech.*, pp. 733-6, Aug. 1971.